Hydrodynamic Stability of Free Convection from an Inclined Elliptic Cylinder

by

Leslie A. Finlay

A thesis

presented to the University of Waterloo

in fulfilment of the

thesis requirement for the degree of

Masters of Mathematics

in

Applied Mathematics

Waterloo, Ontario, Canada, 2006

AUTHOR'S DECLARATION FOR ELECTRONIC

SUBMISSION OF A THESIS

I hereby declare that I am the sole author of this thesis. This is a true copy of the thesis, including any required final revisions, as accepted by my examiners.

I understand that my thesis may be made electronically available to the public.

Abstract

The steady problem of free convective heat transfer from an isothermal inclined elliptic cylinder and its stability is investigated. The cylinder is inclined at an arbitrary angle with the horizontal and immersed in an unbounded, viscous, incompressible fluid. It is assumed that the flow is laminar and two-dimensional and that the Boussinesq approximation is valid. The full steady Navier-Stokes and thermal energy equations are transformed to elliptical coordinates and an asymptotic analysis is used to find appropriate far-field conditions. A numerical scheme based on finite differences is then used to obtain numerical solutions. Results are found for small to moderate Grashof and Prandtl numbers, and varying ellipse inclinations and aspect ratios.

A linear stability analysis is performed to determine the critical Grashof number at which the flow loses stability. Comparisons are made with long-time unsteady solutions.

Acknowledgements

I would first like to thank my supervisor Dr. Serge D'Alessio for his unending encouragement, motivation, and support. I would also like to thank my co-supervisor Dr. J. P. Pascal for his help with the stability analysis. Thanks as well to my examining committee: Dr. Poulin and Dr. Stastna. To my family and friends, thank you.

Contents

List of Figures

Chapter 1

Introduction

1.1 Problem Setup

Unsteady free, or natural, convection from a heated horizontal cylinder is a problem which is interesting to study for both theoretical and practical reasons: a model is generated for studying heat transfer from heated tubes, which is necessary for the design of heat exchangers and other industrial processes.

This thesis investigates the steady state reached by the convection-driven fluid motion around the heated tube, as well as the hydrodynamic stability of the flow. This flow is assumed to be laminar and two-dimensional around the inclined elliptic cylinder, and the fluid is unbounded and otherwise quiescent.

The physical configuration of the problem is illustrated in Figure 1.1. The Cartesian x and y axes are rotated to coincide with the major and minor axes of the ellipse having lengths $2a$ and $2b$, respectively. Gravity acts in the vertical direction, and the ellipse is inclined at an arbitrary angle η measured relative

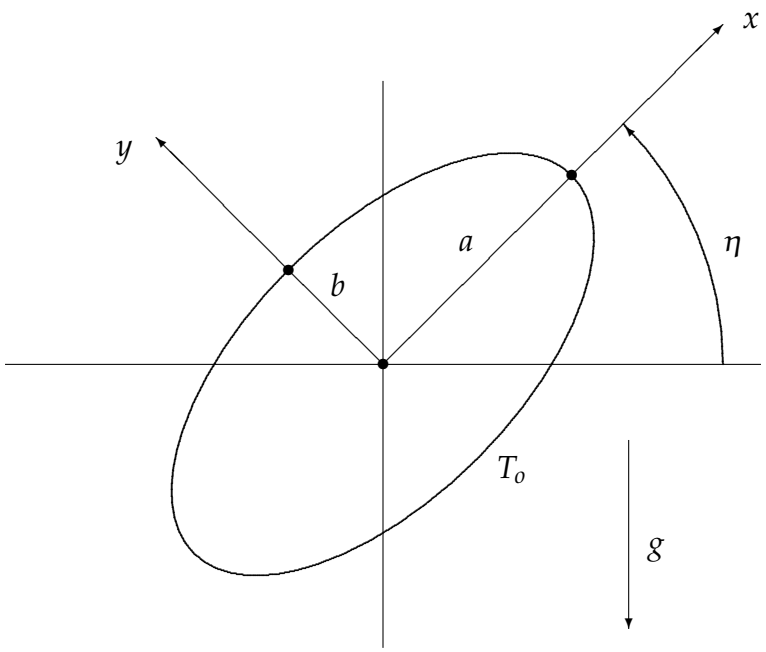

Figure 1.1: Flow Configuration

to the horizontal. The cylinder surface is isothermal with temperature T_0, while the far-field temperature of the fluid is T_∞, with $T_0 > T_\infty$. Throughout this work, the subscript 0 will denote values on the cylinder surface.

This thesis focuses specifically on the steady-state solution to this problem. Once appropriate boundary conditions are found, involving asymptotic analysis of the far-field flow and using Green's Theorem to find integral conditions for the vorticity, the Navier-Stokes equations are solved numerically using finite difference methods. Solutions are found for small to moderate Grashof and Prandtl numbers and various cylinder inclinations and aspect ratios.

As well, a linear stability analysis is performed on the calculated flow to determine if the flow is stable, and if not, at what Grashof number the flow

becomes unstable for a fixed inclination, aspect ratio and Prandtl number. The dependence of flow stability on other variables such as cylinder inclination, aspect ratio, placement of computational outer boundary, and Prandtl number is also examined.

Lastly, a connection with the corresponding unsteady problem is made to contrast the limiting unsteady case with the steady-state case.

1.2 Literature Review

Unsteady free convection from a horizontal cylinder is a fundamental and well-studied problem in thermal fluid mechanics. Numerical, theoretical and experimental work has been performed in this area.

Much attention has been given to the problem of a horizontal cylinder with circular cross-section. Experimental data for flow over a circular cylinder has been compiled by McAdams [13], while Saitoh, Sajiki and Maruhara [16] performed detailed numerical studies of the circular cylinder case with isothermal cylinder surface.

Study of the elliptic tube with major axis oriented to the direction of gravity has also been carried out. Merkin [14] solved the boundary-layer equations for cylinders with the major axis either vertical or horizontal. Results were found for both constant surface temperature and constant heat flux cases. The full unsteady equations are solved by Badr and Shamsher [2], looking at the long-time behaviour for the isothermal cylinder. Experimental study of the

elliptic cylinder has been performed by Elsayed, Ibrahim and Elsayed [10] for tubes with constant heat flux for large Rayleigh numbers, and it can be seen that results from boundary-layer solutions (as in [14]) do not agree well with experimental results in the plume region. Theoretical study of the problem with the cylinder immersed in a non-Newtonian fluid has been carried out by Mahfouz [12].

The problem of mixed convection from an inclined elliptic cylinder has been studied recently by Saunders [17], where the cylinder is taken to have a uniform acceleration. D'Alessio and Harmsworth [5] solved the problem of forced convection from an accelerating cylinder.

D'Alessio and Williams [7] have examined the time development of flow around an elliptic cylinder with different angles of inclination. Badr [1] also studied this problem, and in varying the axis ratios compared results with the limiting cases of the circular cylinder and the flat plate.

The present work extends study of this problem by solving the full governing equations in their steady-state form, comparing results to the long-time unsteady solutions. As well, the stability of the flow is examined.

Chapter 2

Governing Equations

2.1 Derivation

Derivation of the governing equations begins with the continuity equation, taken from Kundu [11]:

$$-\frac{1}{\rho}\frac{D\rho}{Dt} = \nabla \cdot \vec{u}, \tag{2.1}$$

where $\vec{u} = (u, v)$ is the flow velocity with components u in the x-direction and v in the y-direction, and $\frac{D}{Dt} = \frac{\partial}{\partial t} + (\vec{u} \cdot \nabla)$ is the material derivative. The fluid will be assumed to be incompressible, so the continuity equation above simplifies to

$$\nabla \cdot \vec{u} = 0. \tag{2.2}$$

Conservation of momentum for an incompressible fluid is given by the Navier-Stokes equation:

$$\rho\frac{D\vec{u}}{Dt} = -\nabla p + \rho\vec{g} + \mu\nabla^2\vec{u} \tag{2.3}$$

where the gravitational vector $\vec{g} = -g(\sin\eta, \cos\eta)$ and g denotes the gravitational constant.

A constant dynamic viscosity, μ, is assumed, and the Boussinesq approximation ($\rho = \rho_0$ except in gravitational term) is used. These assumptions give the Navier-Stokes equation the form

$$\rho_0 \frac{D\vec{u}}{Dt} = -\nabla p + \rho\vec{g} + \mu\nabla^2\vec{u}. \tag{2.4}$$

We introduce the kinematic viscosity, $\nu = \frac{\mu}{\rho_0}$ and use a linear equation of state as in Kundu [11]:

$$\frac{\rho}{\rho_0} = 1 - \alpha(T - T_\infty) \tag{2.5}$$

where α is the thermal expansion coefficient. Then the Navier-Stokes equation becomes

$$\begin{aligned} \frac{D\vec{u}}{Dt} &= -\frac{1}{\rho_0}\nabla p + \frac{\rho}{\rho_0}\vec{g} + \nu\nabla^2\vec{u} \\ &= -\nabla\left(\frac{p}{\rho_0}\right) + (1 - \alpha(T - T_\infty))\vec{g} + \nu\nabla^2\vec{u} \end{aligned}$$

The vorticity $\vec{\omega}$ is defined by $\vec{\omega} = \nabla \times \vec{u}$, so using the vector identity

$$\nabla \times (\nabla \times \vec{A}) = \nabla(\nabla \cdot \vec{A}) - \nabla^2\vec{A} \tag{2.6}$$

with $\vec{A} = \vec{u}$ gives

$$\nabla \times \vec{\omega} = -\nabla^2\vec{u}$$

by using the continuity equation. Substituting this into the Navier-Stokes equation and expanding the material derivative gives

$$\frac{\partial \vec{u}}{\partial t} + (\vec{u} \cdot \nabla)\vec{u} = -\nabla \left(\frac{p}{\rho_0} \right) + \vec{g} - \alpha \vec{g}(T - T_\infty) - \nu(\nabla \times \vec{\omega}). \tag{2.7}$$

Using a second vector identity

$$(\vec{u} \cdot \nabla)\vec{u} = \frac{1}{2}\nabla(\vec{u} \cdot \vec{u}) - \vec{u} \times \vec{\omega} \tag{2.8}$$

in the Navier-Stokes equation leads to

$$\frac{\partial \vec{u}}{\partial t} - \vec{u} \times \vec{\omega} = -\nabla \left(\frac{p}{\rho_0} + \frac{1}{2}\vec{u} \cdot \vec{u} \right) + \vec{g} - \alpha \vec{g}(T - T_\infty) - \nu(\nabla \times \vec{\omega}). \tag{2.9}$$

Now, the gravitational vector $\vec{g}$ can be written as the gradient of a scalar quantity $\vec{g} = \nabla\Lambda$ if we let

$$\Lambda = -g(x \sin\eta + y \cos\eta).$$

Then if we introduce the quantity Γ as

$$\Gamma = \frac{p}{\rho_0} + \frac{1}{2}\vec{u} \cdot \vec{u} - \Lambda - \alpha T_\infty \Lambda$$

the Navier-Stokes equation becomes

$$\frac{\partial \vec{u}}{\partial t} - \vec{u} \times \vec{\omega} = -\nabla \Gamma - \alpha \vec{g} T - \nu(\nabla \times \vec{\omega}). \tag{2.10}$$

Taking the curl of the previous equation gives

$$\frac{\partial}{\partial t}(\nabla \times \vec{u}) - \nabla \times (\vec{u} \times \vec{\omega}) = -\nabla \times (\nabla \Gamma) - \alpha(\nabla \times \vec{g} T) - \nu(\nabla \times (\nabla \times \vec{\omega})) \tag{2.11}$$

where the first term on the right side is identically zero.

Now, the vector identity

$$\nabla \times (\vec{u} \times \vec{\omega}) = \vec{u}(\nabla \cdot \vec{\omega}) - \vec{\omega}(\nabla \cdot \vec{u}) + (\vec{\omega} \cdot \nabla)\vec{u} - (\vec{u} \cdot \nabla)\vec{\omega} \tag{2.12}$$

simplifies to

$$\nabla \times (\vec{u} \times \vec{\omega}) = -(\vec{u} \cdot \nabla)\vec{\omega} \tag{2.13}$$

because of the continuity equation and the two-dimensionality of the problem. Using this identity and the identity (2.6) with $\vec{A} = \vec{\omega}$, the Navier-Stokes equation has the form

$$\frac{\partial \vec{\omega}}{\partial t} + (\vec{u} \cdot \nabla)\vec{\omega} = -\alpha(\nabla \times \vec{g} T) + \nu \nabla^2 \vec{\omega}. \tag{2.14}$$

The first term on the right side of this equation corresponds to the generation of vorticity due to the baroclinicity of the flow, or generation of vorticity when

surfaces of constant pressure and density are not parallel. The second term on the right represents the change in vorticity due to molecular diffusion.

Because the flow is assumed to be two-dimensional we can introduce a streamfunction, ψ, with

$$u = -\frac{\partial \psi}{\partial y}, \qquad v = \frac{\partial \psi}{\partial x}. \tag{2.15}$$

As well, the vorticity is $\vec{\omega} = \nabla \times \vec{u} = (0, 0, \zeta)$ where

$$\zeta = \frac{\partial v}{\partial x} - \frac{\partial u}{\partial y} = \frac{\partial^2 \psi}{\partial x^2} + \frac{\partial^2 \psi}{\partial y^2}. \tag{2.16}$$

With this definition of the streamfunction, the continuity equation (2.2) is identically satisfied and equation (2.14) becomes the governing equation for the scalar vorticity, ζ.

The first term on the right side of equation (2.14) can be rewritten as

$$\begin{aligned} \nabla \times T\vec{g} &= \nabla \times (-g(T \sin \eta, T \cos \eta, 0)) \\ &= -g \left(0, 0, \cos \eta \frac{\partial T}{\partial x} - \sin \eta \frac{\partial T}{\partial y} \right). \end{aligned}$$

Making this substitution into equation (2.14) yields

$$\frac{\partial \zeta}{\partial t} + (\vec{u} \cdot \nabla)\zeta = \alpha g \left(\cos \eta \frac{\partial T}{\partial x} - \sin \eta \frac{\partial T}{\partial y} \right) + \nu \nabla^2 \zeta. \tag{2.17}$$

Now,

$$\begin{aligned}\vec{u}\cdot\nabla\zeta &= (u,v)\cdot\left(\frac{\partial\zeta}{\partial x},\frac{\partial\zeta}{\partial y}\right)\\ &= \left(-\frac{\partial\psi}{\partial y},\frac{\partial\psi}{\partial x}\right)\cdot\left(\frac{\partial\zeta}{\partial x},\frac{\partial\zeta}{\partial y}\right)\\ &= -\frac{\partial\psi}{\partial y}\frac{\partial\zeta}{\partial x}+\frac{\partial\psi}{\partial x}\frac{\partial\zeta}{\partial y},\end{aligned}$$

which then casts the Navier-Stokes equation (2.17) into the form

$$\frac{\partial\zeta}{\partial t}=\frac{\partial\psi}{\partial x}\frac{\partial\zeta}{\partial y}-\frac{\partial\psi}{\partial x}\frac{\partial\zeta}{\partial y}+\nu\left(\frac{\partial^2\zeta}{\partial x^2}+\frac{\partial^2\zeta}{\partial y^2}\right)+\alpha g\left(\cos\eta\frac{\partial T}{\partial x}-\sin\eta\frac{\partial T}{\partial y}\right). \tag{2.18}$$

An equation governing the fluid temperature is also needed. The thermal energy equation to be used is

$$\rho\frac{De}{Dt}=-\nabla\cdot\vec{q}-p(\nabla\cdot\vec{u})+\varepsilon \tag{2.19}$$

where e is the internal energy of the fluid, $\vec{q}$ is the heat flux per unit area, and ε is the viscous dissipation. For the cases considered in this thesis, viscous dissipation is expected to be negligible, thus the term ε will be dropped.

The internal energy and heat flux per unit area can be written in terms of the fluid temperature using

$$e=C_pT,\qquad \vec{q}=-k\nabla T$$

where C_p and k are the specific heat at constant pressure, and thermal con-

ductivity of the fluid, respectively.

Now, for constant C_p,

$$\rho \frac{DC_pT}{Dt} = \rho C_p \frac{DT}{Dt}$$

and for constant k,

$$-\nabla \cdot \vec{q} = -\nabla(-k\nabla T) = k\nabla^2 T.$$

Making these substitutions into the thermal energy equation (2.19) and using the continuity equation (2.2) gives the temperature equation

$$\rho C_p \frac{DT}{Dt} = k\nabla^2 T. \tag{2.20}$$

We introduce the thermal diffusivity κ, defined by $\kappa = \frac{k}{\rho C_p}$.

The material derivative in (2.20) gives

$$\begin{aligned} \frac{DT}{Dt} &= \frac{\partial T}{\partial t} + \vec{u} \cdot \nabla T \\ &= \frac{\partial T}{\partial t} + \left(-\frac{\partial \psi}{\partial y}, \frac{\partial \psi}{\partial x} \right) \cdot \left(\frac{\partial T}{\partial x}, \frac{\partial T}{\partial y} \right) \\ &= \frac{\partial T}{\partial t} - \frac{\partial \psi}{\partial y}\frac{\partial T}{\partial x} + \frac{\partial \psi}{\partial x}\frac{\partial T}{\partial y} \end{aligned}$$

which transforms the temperature equation to

$$\frac{\partial T}{\partial t} = \frac{\partial \psi}{\partial y}\frac{\partial T}{\partial x} - \frac{\partial \psi}{\partial x}\frac{\partial T}{\partial y} + \kappa\nabla^2 T. \tag{2.21}$$

2.2 Non-Dimensionalization

To non-dimensionalize the governing equations (2.16), (2.18), and (2.21) we use a length scale given by $c = \sqrt{a^2 - b^2}$, the semi-focal length of the ellipse, a time scale of $\frac{c^2}{\nu}$, and a temperature scale based on the difference between T_0 and T_∞. Thus, the change of variables to be used is

$$\begin{aligned} \tilde{x} &= \frac{x}{c}, \qquad \tilde{y} = \frac{y}{c}, \\ \tilde{t} &= \frac{\nu}{c^2} t, \qquad \tilde{\psi} = \frac{1}{\nu}\psi, \\ \tilde{\zeta} &= \frac{c^2}{\nu}\zeta, \qquad \phi = \frac{T - T_\infty}{T_0 - T_\infty}, \end{aligned} \tag{2.22}$$

where the tilded variables, as well as ϕ, are dimensionless.

We also introduce two additional dimensionless parameters: the Grashof number Gr and the Prandtl number Pr, given by

$$Gr = \frac{\alpha g c^3 (T_0 - T_\infty)}{\nu^2} \quad \text{and} \quad Pr = \frac{\nu}{\kappa}.$$

The Grashof number represents the relative strength of the buoyancy forces to the viscous forces, while the Prandtl number is the ratio of momentum diffusivity to thermal diffusivity of the fluid.

Making these substitutions into the governing equations and dropping the tildes for ease of notation leads to the following set of equations: the stream-

function equation

$$\frac{\partial^2 \psi}{\partial x^2} + \frac{\partial^2 \psi}{\partial y^2} = \zeta, \tag{2.23}$$

the vorticity equation

$$\frac{\partial \zeta}{\partial t} = \frac{\partial^2 \zeta}{\partial x^2} + \frac{\partial^2 \zeta}{\partial y^2} - \frac{\partial \psi}{\partial x}\frac{\partial \zeta}{\partial y} + \frac{\partial \psi}{\partial y}\frac{\partial \zeta}{\partial x} + Gr\left(\cos\eta \frac{\partial \phi}{\partial x} - \sin\eta \frac{\partial \phi}{\partial y}\right), \tag{2.24}$$

and the heat equation

$$\frac{\partial \phi}{\partial t} = \frac{1}{Pr}\left(\frac{\partial^2 \phi}{\partial x^2} + \frac{\partial^2 \phi}{\partial y^2}\right) + \frac{\partial \psi}{\partial y}\frac{\partial \phi}{\partial x} - \frac{\partial \psi}{\partial x}\frac{\partial \phi}{\partial y}. \tag{2.25}$$

2.3 Transformation to Elliptical Co-ordinates

For ease of computation, a conformal map is used to change to elliptical co-ordinates as shown in Figure 2.1. The mapping is given by

$$x + iy = \cosh\left[(\xi + \xi_0) + i\theta\right], \tag{2.26}$$

where $\tanh\xi_0 = r$, and $r = b/a$ is the ratio of the semi-minor and semi-major axis lengths. Using the identity $\cosh z = \frac{1}{2}\left(e^z + e^{-z}\right)$ and equating the real and imaginary parts of equation (2.26) gives

$$x = \cosh\left(\xi + \xi_0\right)\cos\theta, \qquad y = \sinh\left(\xi + \xi_0\right)\sin\theta. \tag{2.27}$$

The scale factors for this transformation are given by

$$h_\xi = \sqrt{\left(\frac{\partial x}{\partial \xi}\right)^2 + \left(\frac{\partial y}{\partial \xi}\right)^2}, \qquad h_\theta = \sqrt{\left(\frac{\partial x}{\partial \theta}\right)^2 + \left(\frac{\partial y}{\partial \theta}\right)^2}.$$

Using equation (2.27) leads to

$$h_\xi = \sqrt{\cosh^2(\xi + \xi_0) - \cos^2\theta}, \qquad h_\theta = \sqrt{\cosh^2(\xi + \xi_0) - \cos^2\theta}.$$

The metric of the transformation, $M(\xi, \theta) = h_\xi = h_\theta$, can then be expressed by

$$\begin{aligned} M^2(\xi,\theta) &= \cosh^2(\xi + \xi_0) - \cos^2\theta \\ &= \frac{1}{2}\left[\cosh 2(\xi + \xi_0) - \cos 2\theta\right]. \end{aligned} \tag{2.28}$$

For the remainder of this thesis the dependence of M on ξ and θ will be implied.

Differentiating equations (2.27) with respect to x and y and solving the resulting equations gives

$$\frac{\partial \xi}{\partial x} = \frac{1}{M^2}\sinh(\xi + \xi_0)\cos\theta, \tag{2.29}$$

$$\frac{\partial \xi}{\partial y} = \frac{1}{M^2}\cosh(\xi + \xi_0)\sin\theta, \tag{2.30}$$

$$\frac{\partial \theta}{\partial x} = -\frac{1}{M^2}\cosh(\xi + \xi_0)\sin\theta, \tag{2.31}$$

$$\frac{\partial \theta}{\partial y} = \frac{1}{M^2}\sinh(\xi + \xi_0)\cos\theta. \tag{2.32}$$

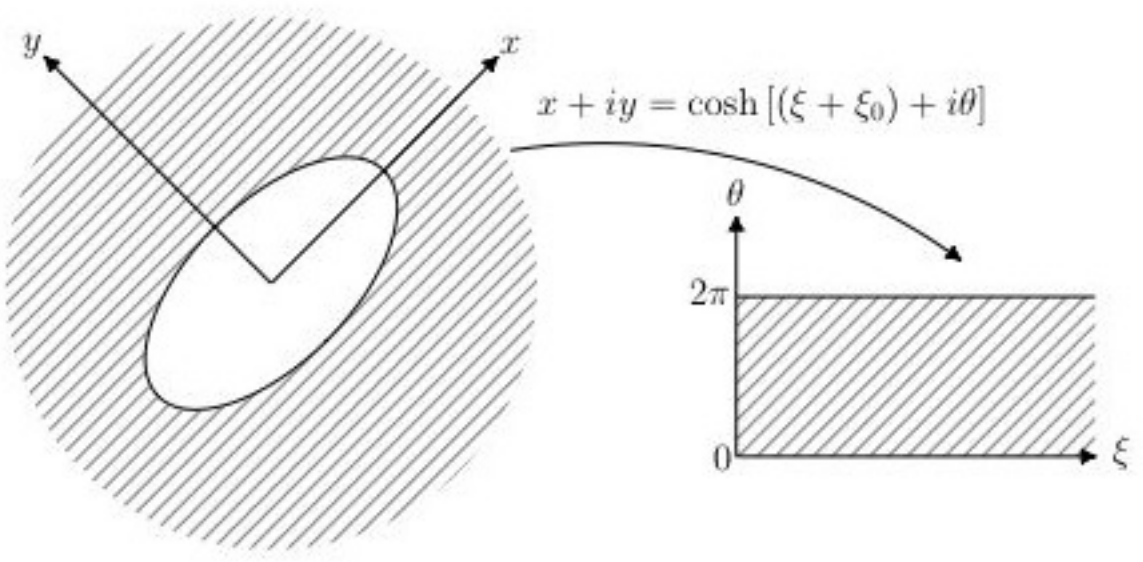

Figure 2.1: Transformation from cartesian to elliptical co-ordinates

Differentiating equations (2.29)-(2.32) gives

$$\frac{\partial^2 \xi}{\partial x^2} = \frac{\sinh(\xi+\xi_0)\cosh(\xi+\xi_0)}{M^4}\left[1 - \frac{2\cos^2\theta\left(\sinh^2(\xi+\xi_0) - \sin^2\theta\right)}{M^2}\right] \quad (2.33)$$

$$\frac{\partial^2 \xi}{\partial y^2} = \frac{\sinh(\xi+\xi_0)\cosh(\xi+\xi_0)}{M^4}\left[1 - \frac{2\sin^2\theta\left(\cosh^2(\xi+\xi_0) - \cos^2\theta\right)}{M^2}\right] \quad (2.34)$$

$$\frac{\partial^2 \theta}{\partial x^2} = \frac{\sin\theta\cos\theta}{M^4}\left[1 + \frac{2\cosh^2(\xi+\xi_0)\left(\sinh^2(\xi+\xi_0) - \sin^2\theta\right)}{M^2}\right], \quad (2.35)$$

$$\frac{\partial^2 \theta}{\partial y^2} = \frac{\sin\theta\cos\theta}{M^4}\left[1 - \frac{2\sinh^2(\xi+\xi_0)\left(\cosh^2(\xi+\xi_0) - \cos^2\theta\right)}{M^2}\right]. \quad (2.36)$$

The chain rule for differentiation is

$$\begin{aligned}\frac{\partial \Omega}{\partial x_i} &= \frac{\partial \Omega}{\partial \xi}\frac{\partial \xi}{\partial x_i} + \frac{\partial \Omega}{\partial \theta}\frac{\partial \theta}{\partial x_i}, \\ \frac{\partial^2 \Omega}{\partial x_i^2} &= \frac{\partial^2 \Omega}{\partial \xi^2}\left(\frac{\partial \xi}{\partial x_i}\right)^2 + \frac{\partial \Omega}{\partial \xi}\frac{\partial^2 \xi}{\partial x_i^2} + \frac{\partial^2 \Omega}{\partial \theta^2}\left(\frac{\partial \theta}{\partial x_i}\right)^2 + \frac{\partial \Omega}{\partial \theta}\frac{\partial^2 \theta}{\partial x_i^2},\end{aligned}$$

where Ω is one of ϕ, ψ, or ζ and x_i is either x or y. Using these derivative formulae with the derivatives (2.29)-(2.36), the streamfunction equation (2.23) becomes

$$\frac{\partial^2 \psi}{\partial \xi^2} + \frac{\partial^2 \psi}{\partial \theta^2} = M^2 \zeta. \tag{2.37}$$

The vorticity equation (2.24) can be written as

$$\frac{\partial \zeta}{\partial t} = \frac{1}{M^2}\left[-\frac{\partial \psi}{\partial \xi}\frac{\partial \zeta}{\partial \theta} + \frac{\partial \psi}{\partial \theta}\frac{\partial \zeta}{\partial \xi} + \frac{\partial^2 \zeta}{\partial \xi^2} + \frac{\partial^2 \zeta}{\partial \theta^2} + Gr\left(A(\xi,\theta)\frac{\partial \phi}{\partial \xi} - B(\xi,\theta)\frac{\partial \phi}{\partial \theta}\right)\right], \tag{2.38}$$

where the functions $A(\xi,\theta)$ and $B(\xi,\theta)$ are introduced for brevity and are defined as

$$A(\xi,\theta) = \sinh(\xi+\xi_0)\cos(\eta)\cos(\theta) - \cosh(\xi+\xi_0)\sin(\eta)\sin(\theta), \tag{2.39}$$

$$B(\xi,\theta) = \cosh(\xi+\xi_0)\cos(\eta)\sin(\theta) + \sinh(\xi+\xi_0)\sin(\eta)\cos(\theta). \tag{2.40}$$

Finally, the heat equation (2.25) takes the form

$$\frac{\partial \phi}{\partial t} = \frac{1}{M^2}\left[-\frac{\partial \psi}{\partial \xi}\frac{\partial \phi}{\partial \theta} + \frac{\partial \psi}{\partial \theta}\frac{\partial \phi}{\partial \xi} + \frac{1}{Pr}\left(\frac{\partial^2 \phi}{\partial \xi^2} + \frac{\partial^2 \phi}{\partial \theta^2}\right)\right]. \tag{2.41}$$

Equations (2.37), (2.38), and (2.41) give the full unsteady governing equations for the system. This work requires the steady-state equations, which are found by setting the time derivatives to zero in the previous equations. The streamfunction equation (2.37) then remains the same, and the vorticity and heat equations become

$$\frac{\partial^2\zeta}{\partial\xi^2}+\frac{\partial^2\zeta}{\partial\theta^2}=\frac{\partial\psi}{\partial\xi}\frac{\partial\zeta}{\partial\theta}-\frac{\partial\psi}{\partial\theta}\frac{\partial\zeta}{\partial\xi}-Gr(A\frac{\partial\phi}{\partial\xi}-B\frac{\partial\phi}{\partial\theta}), \tag{2.42}$$

and

$$\frac{\partial^2\phi}{\partial\xi^2}+\frac{\partial^2\phi}{\partial\theta^2}=Pr(\frac{\partial\psi}{\partial\xi}\frac{\partial\phi}{\partial\theta}-\frac{\partial\psi}{\partial\theta}\frac{\partial\phi}{\partial\xi}), \tag{2.43}$$

respectively.

2.4 Boundary Conditions

In order to solve the governing steady-state equations found in the previous section, boundary conditions are required. On the cylinder surface ($\xi = 0$) the conditions needed are no-slip along the surface, no flow through the surface, and constant temperature at the surface. To institute the no-slip and impermeability conditions it is useful to express the flow velocity in terms of the streamfunction, ψ.

The flow velocity can be written as $\vec{u} = (u_\xi, u_\theta)$ where u_ξ is the ξ-component of the velocity and u_θ the θ-component. Then the no-slip condition corresponds

to

$$u_\theta = 0 \quad \text{on} \quad \xi = 0 \tag{2.44}$$

and the impermeability condition corresponds to

$$u_\xi = 0 \quad \text{on} \quad \xi = 0. \tag{2.45}$$

To express the velocity components in terms of the streamfunction we recall that the divergence in curvilinear co-ordinates is given by

$$\nabla \cdot \vec{u} = \frac{1}{h_\xi h_\theta}\left[\frac{\partial(h_\theta u_\xi)}{\partial \xi} + \frac{\partial(h_\xi u_\theta)}{\partial \theta}\right], \tag{2.46}$$

and when substituted in the continuity equation (2.2) this can be written as

$$\frac{1}{M^2}\left[\frac{\partial(M u_\xi)}{\partial \xi} + \frac{\partial(M u_\theta)}{\partial \theta}\right] = 0. \tag{2.47}$$

Now ψ can be defined in the (ξ, θ)-plane such that

$$M u_\xi = -\frac{\partial \psi}{\partial \theta}, \qquad M u_\theta = \frac{\partial \psi}{\partial \xi},$$

which automatically satisfies equation (2.47). Rearranging the previous equations then gives the velocity components in terms of the streamfunction as

$$u_\xi = -\frac{1}{M}\frac{\partial \psi}{\partial \theta}, \qquad u_\theta = \frac{1}{M}\frac{\partial \psi}{\partial \xi}. \tag{2.48}$$

The impermeability condition (2.45), when written in terms of the streamfunction, then becomes

$$\frac{\partial \psi}{\partial \theta} = 0 \quad \text{on} \quad \xi = 0.$$

This gives ψ equal to a constant on the cylinder surface. Since there is only one solid boundary, without loss of generality, we can set this constant to zero.

The no-slip condition (2.44) when written in terms of the streamfunction and combined with the impermeability condition gives

$$\psi = \frac{\partial \psi}{\partial \xi} = 0 \quad \text{on} \quad \xi = 0. \tag{2.49}$$

The condition on the temperature, $T = T_0$, gives, from equation (2.22),

$$\phi = \frac{T_0 - T_\infty}{T_0 - T_\infty} = 1 \quad \text{on} \quad \xi = 0. \tag{2.50}$$

We now have conditions on the cylinder surface for the streamfunction and temperature. In the next section it will be shown that the vorticity satisfies integral, or global, conditions.

Far from the cylinder surface we have quiescent flow, which corresponds to

$$u_\xi, u_\theta \to 0 \quad \text{as} \quad \xi \to \infty. \tag{2.51}$$

From the definition of the streamfunction, the above condition implies that

$$\frac{\partial \psi}{\partial \xi}, \qquad \frac{\partial \psi}{\partial \theta} \to 0 \quad \text{as} \quad \xi \to \infty. \tag{2.52}$$

This will be satisfied if the streamfunction approaches a constant $\psi = \psi_\infty$. We need this constant to be the same as the value of the streamfunction on the cylinder surface, thus

$$\psi \to 0 \quad \text{as} \quad \xi \to \infty.$$

Using the vorticity equation (2.42), it is seen that the far-field condition for the vorticity is

$$\zeta \to 0 \quad \text{as} \quad \xi \to \infty.$$

For the temperature we have

$$T \to T_\infty \quad \text{as} \quad \xi \to \infty,$$

which corresponds to

$$\phi \to \frac{T_\infty - T_\infty}{T_0 - T_\infty} = 0 \quad \text{as} \quad \xi \to \infty. \tag{2.53}$$

Thus we have the far-field conditions

$$\psi, \zeta, \phi \to 0 \quad \text{as} \quad \xi \to \infty. \tag{2.54}$$

Using asymptotic analysis we can determine more mathematically appropriate far-field conditions; such an analysis will be carried out in a future section.

2.5 Integral Conditions

The vorticity field can be shown to satisfy integral conditions which are derived by using Green's second identity:

$$\int\int_D (g\nabla^2 h - h\nabla^2 g)\,\mathrm{d}A = \oint_C (g\frac{\partial h}{\partial \vec{n}} - h\frac{\partial g}{\partial \vec{n}})\,\mathrm{d}S, \tag{2.55}$$

where D is the fluid domain, C is the closed curve surrounding the domain D, and $\frac{\partial}{\partial \vec{n}}$ represents the normal derivative.

We let $g = \psi$ and $h = e^{-n\xi}\left\{\begin{array}{c}\sin(n\theta)\\ \\ \cos(n\theta)\end{array}\right\}$ for $n = 0, 1, 2, \cdots$. Then in the interior of the integration domain, by using the streamfunction equation (2.37), we have

$$\nabla^2 g = \nabla^2 \psi = M^2 \zeta, \tag{2.56}$$

$$\nabla^2 h = 0. \tag{2.57}$$

On the solid boundary

$$g = \psi = 0, \tag{2.58}$$

$$\frac{\partial g}{\partial \vec{n}} = \frac{\partial \psi}{\partial \xi} = 0. \tag{2.59}$$

In the far field,

$$h \sim e^{-n\xi} \to 0, \quad n \neq 0, \tag{2.60}$$

$$\frac{\partial h}{\partial \vec{n}} = \frac{\partial h}{\partial \xi} \to 0. \tag{2.61}$$

Substituting the above into equation (2.55) leads to the integral conditions

$$\int_0^\infty \int_0^{2\pi} e^{-n\xi} M^2 \zeta \left\{ \begin{array}{c} \sin(n\theta) \\ \\ \cos(n\theta) \end{array} \right\} \mathrm{d}\theta \, \mathrm{d}\xi = 0 \quad n = 0, 1, 2, \cdots . \tag{2.62}$$

By using the known boundary conditions these integral constraints could be used to find the vorticity throughout the domain, as can be seen in [8], but such an approach is computationally difficult with the strong possibility of convergence problems, and so is not practical. The integral conditions, however, can be useful in finding a formula for the surface vorticity, as well as the far-field condition for the vorticity. Both of these will be examined in later sections.

Chapter 3

Analytical Solutions

In solving the steady-state problem the far-field conditions $\psi, \zeta, \phi \to 0$ as $\xi \to \infty$ are imposed. Computationally, the outer boundary ξ_∞ is used to approximate infinity. As a compromise between computational efficiency and mathematical correctness it is desirable to derive more appropriate conditions that can be applied along the boundary ξ_∞. One approach in obtaining these far-field conditions is to make use of the well-known similarity solution from a line heat source (as in [4]), since at large distances the cylinder can be viewed as a line. While this approach seems promising there are serious drawbacks. For example, the similarity solution is based on the boundary-layer equations and for small to moderate Grashof numbers considered here, the validity of these equations is questionable. Further, as pointed out by Suriano and Yang [18], the vertical velocity predicted by the similarity solution increases without bound with distance from the source and this behaviour is clearly not physical. For these reasons a different approach was adopted. Although the analysis

outlined below is not rigorous, it is more than adequate for our numerical purposes.

3.1 Asymptotic Analysis

By examining the far-field behaviour of the streamfunction, vorticity, and temperature, more appropriate conditions than those in (2.54) can be established.

As a first far-field approximation of equations (2.37), (2.42), and (2.43), one is tempted to solve

$$\nabla^2 \psi = 0, \tag{3.1}$$

$$\nabla^2 \zeta = 0, \tag{3.2}$$

$$\nabla^2 \phi = 0. \tag{3.3}$$

The solutions to (3.1) - (3.3) satisfying the far-field conditions (2.54) are:

$$\psi, \zeta, \phi \sim e^{-n\xi} \left\{ \begin{array}{c} \sin(n\theta) \\ \\ \cos(n\theta) \end{array} \right\} \quad \forall n \in \mathbf{Z}^+, \quad \text{as} \quad \xi \to \infty. \tag{3.4}$$

The leading order term ($n = 1$) for ψ represents an improved approximation for the far-field behaviour of the streamfunction and can be expressed as

$$\psi \sim a_1 e^{-\xi} \cos(\theta - \alpha_1). \tag{3.5}$$

where a_1 and α_1 are arbitrary constants.

Then the vorticity equation (2.42) for large ξ has the form

$$\nabla^2\zeta - a_1 e^{-\xi}\left(-\cos(\theta-\alpha_1)\frac{\partial\zeta}{\partial\theta} + \sin(\theta-\alpha_1)\frac{\partial\zeta}{\partial\xi}\right) = \\ -\frac{Gr}{2}e^{\xi}\left(\cos(\theta+\eta)\frac{\partial\phi}{\partial\xi} - \sin(\theta+\eta)\frac{\partial\phi}{\partial\theta}\right). \tag{3.6}$$

We will examine the homogeneous form of (3.6) by setting the right side to equal zero. To solve this equation we set

$$\zeta = e^{F(\xi,\theta)}\hat{\zeta}(\xi,\theta), \tag{3.7}$$

and with

$$F(\xi,\theta) = -\frac{a_1}{2}e^{-\xi}\sin(\theta-\alpha_1) \tag{3.8}$$

the first derivatives in (3.6) are eliminated, giving the transformed equation for $\hat{\zeta}$

$$\nabla^2\hat{\zeta} - \frac{1}{4}e^{-2\xi}\hat{\zeta} = 0. \tag{3.9}$$

Separation of variables $\hat{\zeta} = P(\xi)Q(\theta)$ leads to

$$Q_n''(\theta) + n^2 Q_n(\theta) = 0 \tag{3.10}$$

$$\Rightarrow Q_n(\theta) = p_n\sin(n\theta) + q_n\cos(n\theta), \quad p_n, q_n \in \mathbf{R} \tag{3.11}$$

and, letting $z = \frac{a_1}{2}e^{-\xi}$ gives

$$z^2 P_n''(z) + z P_n'(z) - (z^2 + n^2) P_n(z) = 0 \tag{3.12}$$

$$\Rightarrow P_n(z) = c_n I_n(z) + d_n K_n(z) \quad c_n, d_n \in \mathbf{R} \tag{3.13}$$

where $I_n(z), K_n(z)$ are the modified Bessel functions of the first and second kind, respectively.

We are looking for the far-field behaviour, and since $z \to 0$ as $\xi \to \infty$ by definition of z, we examine the limits of the modified Bessel functions as the argument approaches zero.

Since $K_n(z) \to \infty$ as $z \to 0$, we set $d_n = 0$.

The small-argument expansion of the modified Bessel function of the first kind is

$$I_n(z) \sim \frac{(\frac{z}{2})^n}{n!} \quad \text{as} \quad z \to 0. \tag{3.14}$$

Then from equation (3.13)

$$P_n(z) \sim \frac{c_n(\frac{z}{2})^n}{n!} \quad \text{as} \quad z \to 0 \tag{3.15}$$

$$\Rightarrow P_n(\xi) \sim \tilde{c}_n e^{-n\xi} \quad \text{as} \quad \xi \to \infty \tag{3.16}$$

where

$$\tilde{c}_n = \frac{c_n a_1^n}{4^n n!} \in \mathbf{R}. \tag{3.17}$$

Then equations (3.11) and (3.16) give the solution to the PDE for $\hat{\zeta}$, (3.9):

$$\hat{\zeta}(\xi,\theta) = \sum_{n=1}^{\infty} e^{-n\xi}[p_n \sin(n\theta) + q_n \cos(n\theta)], \quad p_n, q_n \in \mathbf{R}. \tag{3.18}$$

Now the leading order term needs to be determined. This is done by recalling the integral condition

$$\int_0^{\infty}\int_0^{2\pi} e^{-n\xi} M^2 \zeta \left\{ \begin{array}{c} \sin(n\theta) \\ \\ \cos(n\theta) \end{array} \right\} \mathrm{d}\theta\, \mathrm{d}\xi = 0 \quad n = 0, 1, 2, \cdots .$$

Taking the $n = 0$ case gives

$$\int_0^{\infty}\int_0^{2\pi} M^2 \zeta \,\mathrm{d}\theta\, \mathrm{d}\xi = 0. \tag{3.19}$$

From equation (2.28) it is clear that for large ξ, $M^2 \sim e^{2\xi}$, and we have $\zeta \to \hat{\zeta}$ as $\xi \to \infty$, so for convergence of the integral in equation (3.19) the vorticity must decay no slower than

$$\hat{\zeta} \sim a_2 e^{-3\xi} \cos(3\theta - \alpha_2) \quad \text{as} \quad \xi \to \infty. \tag{3.20}$$

With this form of $\hat{\zeta}$, by equation (3.7) we have

$$\zeta = a_2 e^{-3\xi} \cos(3\theta - \alpha_2) e^{F(\xi,\theta)}$$

where $F(\xi,\theta)$ is given in equation (3.8).

Looking at the Taylor expansion of e^F gives

$$e^{F(\xi,\theta)} \approx 1 - \frac{a_1}{2} e^{-\xi} \sin(\theta - \alpha) + \cdots ,$$

which gives us, to leading order,

$$\zeta \sim a_2 e^{-3\xi} \cos(3\theta - \alpha_2).$$

Now looking for the asymptotic form of the temperature, we see that the heat equation (2.43), with (3.5), has the form

$$\nabla^2 \phi - a_1 \, Pr \, e^{-\xi} \left(- \cos(\theta - \alpha_1) \frac{\partial \phi}{\partial \theta} + \sin(\theta - \alpha_1) \frac{\partial \phi}{\partial \xi} \right) = 0 \tag{3.21}$$

which is similar to the homogeneous form of (3.6). Thus we expect the solution for ϕ to have the same form as that for ζ:

$$\phi(\xi, \theta) = \sum_{n=1}^{\infty} e^{-n\xi} [p'_n \sin(n\theta) + q'_n \cos(n\theta)], \quad p'_n, q'_n \in \mathbf{R}. \tag{3.22}$$

In order to guarantee that the right side of equation (3.6) is at most of order $e^{-3\xi}$ we need to have the leading term in (3.22) behave as

$$\phi \sim a_3 e^{-4\xi} \cos(4\theta - \alpha_3) \quad \text{as} \quad \xi \to \infty. \tag{3.23}$$

In summary, the far-field conditions for the streamfunction, vorticity and

heat are

$$\psi \sim a_1 e^{-\xi} \cos(\theta - \alpha_1) \quad \text{as} \quad \xi \to \infty, \tag{3.24}$$

$$\zeta \sim a_2 e^{-3\xi} \cos(3\theta - \alpha_2) \quad \text{as} \quad \xi \to \infty, \tag{3.25}$$

$$\phi \sim a_3 e^{-4\xi} \cos(4\theta - \alpha_3) \quad \text{as} \quad \xi \to \infty. \tag{3.26}$$

3.2 Linear Stability Analysis

The linear stability analysis, which follows methods found in Drazin and Reid [9], begins with the governing unsteady equations, (2.37), (2.38), and (2.41). The streamfunction equation is easily eliminated from this system by substituting (2.37) into equation (2.38), giving

$$\begin{aligned} \frac{\partial}{\partial t}\nabla^2\psi = &-\frac{\partial\psi}{\partial\xi}\frac{\partial}{\partial\theta}\left(\frac{1}{M^2}\nabla^2\psi\right) + \frac{\partial\psi}{\partial\theta}\frac{\partial}{\partial\xi}\left(\frac{1}{M^2}\nabla^2\psi\right) \\ &+ \nabla^2\left(\frac{1}{M^2}\nabla^2\psi\right) + Gr\left(A\frac{\partial\phi}{\partial\xi} - B\frac{\partial\phi}{\partial\theta}\right). \end{aligned} \tag{3.27}$$

Perturbations are introduced into the flow variables:

$$\psi = \psi_s + \psi', \quad \phi = \phi_s + \phi'$$

where ψ_s and ϕ_s are the solutions of the steady-state equations (so $\frac{\partial\psi_s}{\partial t} = \frac{\partial\phi_s}{\partial t} = 0$) and ψ' and ϕ' are small perturbations. Looking first at

equation (2.41) we get

$$\begin{aligned}\frac{\partial \phi'}{\partial t} &= \frac{1}{M^2}\left[-\left(\frac{\partial \psi_s}{\partial \xi}\frac{\partial \phi_s}{\partial \theta}+\frac{\partial \psi_s}{\partial \xi}\frac{\partial \phi'}{\partial \theta}+\frac{\partial \psi'}{\partial \xi}\frac{\partial \phi_s}{\partial \theta}+\frac{\partial \psi'}{\partial \xi}\frac{\partial \phi'}{\partial \theta}\right)\right.\\ &\quad\left.+\left(\frac{\partial \psi_s}{\partial \theta}\frac{\partial \phi_s}{\partial \xi}+\frac{\partial \psi_s}{\partial \theta}\frac{\partial \phi'}{\partial \xi}+\frac{\partial \psi'}{\partial \theta}\frac{\partial \phi_s}{\partial \xi}+\frac{\partial \phi'}{\partial \theta}\frac{\partial \phi'}{\partial \xi}\right)+\frac{1}{Pr}\nabla^2\phi_s+\frac{1}{Pr}\nabla^2\phi'\right].\end{aligned}$$

This equation is linearized by dropping the terms which are of second order in the perturbations. As well, since ψ_s and ϕ_s are solutions to the steady-state equations (2.42) and (2.43) these can be used to simplify the above stability equation. After this linearization and simplification, we find the temperature perturbation equation to be

$$\frac{\partial \phi'}{\partial t} = \frac{1}{M^2}\left[-\frac{\partial \psi_s}{\partial \xi}\frac{\partial \phi'}{\partial \theta}-\frac{\partial \psi'}{\partial \xi}\frac{\partial \phi_s}{\partial \theta}+\frac{\partial \psi_s}{\partial \theta}\frac{\partial \phi'}{\partial \xi}+\frac{\partial \psi'}{\partial \theta}\frac{\partial \phi_s}{\partial \xi}+\frac{1}{\mathrm{Pr}}\nabla^2\phi'\right]. \tag{3.28}$$

Following the same steps with equation (3.27) gives the vorticity perturbation equation

$$\begin{aligned}\frac{\partial}{\partial t}\left(\nabla^2\psi'\right) &= -\frac{\partial \psi_s}{\partial \xi}\frac{\partial}{\partial \theta}\left(\frac{1}{M^2}\nabla^2\psi'\right)-\frac{\partial \psi'}{\partial \xi}\frac{\partial}{\partial \theta}\left(\frac{1}{M^2}\nabla^2\psi_s\right)+\frac{\partial \psi_s}{\partial \theta}\frac{\partial}{\partial \xi}\left(\frac{1}{M^2}\nabla^2\psi'\right)\\ &\quad+\frac{\partial \psi'}{\partial \theta}\frac{\partial}{\partial \xi}\left(\frac{1}{M^2}\nabla^2\psi_s\right)+\nabla^2\left(\frac{1}{M^2}\nabla^2\psi'\right)+Gr\left(A\frac{\partial \phi'}{\partial \xi}-B\frac{\partial \phi'}{\partial \theta}\right).\end{aligned} \tag{3.29}$$

To make this problem more tractable, we simplify the above equations: the coefficients in equations (3.28) and (3.29) are integrated with respect to θ from 0 to 2π to remove the θ-dependence.

Because of the simplified version of the equations, we can now assume two-

dimensional normal mode disturbances of the form

$$\psi'(\xi,\theta,t) = F_m(\xi)e^{-im\theta}e^{\sigma t}, \quad \phi'(\xi,\theta,t) = G_m(\xi)e^{-im\theta}e^{\sigma t} \tag{3.30}$$

where m is a positive integer indicating the mode of the disturbance, and σ is the complex-valued growth rate. If

$$\text{Real}(\sigma) > 0$$

then the system has an instability, while if

$$\text{Real}(\sigma) < 0$$

then the system is stable.

Given these forms of the disturbances, we now have a pair of ordinary differential equations:

$$G_m'' + g_1 G_m = g_2 F_m, \tag{3.31}$$

$$F_m'''' + f_1 F_m''' + f_2 F_m'' + f_3 F_m' + f_4 F_m = 0, \tag{3.32}$$

where the prime denotes differentiation with respect to ξ and the coefficients

$g_1, g_2, f_1, f_2, f_3, f_4$ are functions of ξ defined by

$$
\begin{aligned}
f_1 &= -4, \\
f_2(\xi) &= -2m^2 - 4 - \frac{\sigma}{2}\cosh\left[2(\xi+\xi_0)\right] + \frac{8\cosh\left[2(\xi+\xi_0)\right]}{\sinh\left[2(\xi+\xi_0)\right]} + \frac{im}{2\pi}\int_0^{2\pi}\frac{\partial\psi_s}{\partial\xi}\,\mathrm{d}\theta \\
&\quad + \frac{1}{2\pi}\int_0^{2\pi}\frac{\sin(2\theta)}{M^2}\frac{\partial\psi_s}{\partial\xi}\,\mathrm{d}\theta, \\
f_3(\xi) &= 4m^2 + \frac{1}{2\pi}\int_0^{2\pi}\zeta_s\sin(2\theta)\,\mathrm{d}\theta, \\
f_4(\xi) &= m^4 + 4m^2 + \frac{\sigma m^2}{2}\cosh\left[2(\xi+\xi_0)\right] - \frac{8m^2\cosh\left[2(\xi+\xi_0)\right]}{\sinh\left[2(\xi+\xi_0)\right]} \\
&\quad - \frac{im^3}{2\pi}\int_0^{2\pi}\frac{\partial\psi_s}{\partial\xi}\,\mathrm{d}\theta - \frac{im}{2\pi}\int_0^{2\pi}M^2\frac{\partial\zeta_s}{\partial\xi}\,\mathrm{d}\theta - \frac{m^2}{2\pi}\int_0^{2\pi}\frac{\sin(3\theta)}{M^2}\frac{\partial\psi_s}{\partial\xi}\,\mathrm{d}\theta \\
&\quad + \frac{m^2\sinh\left[2(\xi+\xi_0)\right]}{2\pi}\int_0^{2\pi}\frac{\psi_s\sin(2\theta)}{M^4}\,\mathrm{d}\theta, \\
g_1(\xi) &= -m^2 - \frac{\sigma Pr}{2}\cosh\left[2(\xi+\xi_0)\right] + \frac{imPr}{2\pi}\int_0^{2\pi}\frac{\partial\psi_s}{\partial\xi}\,\mathrm{d}\theta, \\
g_2(\xi) &= \frac{imPr}{2\pi}\int_0^{2\pi}\frac{\partial\phi_s}{\partial\xi}\,\mathrm{d}\theta.
\end{aligned}
$$

These coefficients have been simplified using the following integration results

$$\int_0^{2\pi} M^2\,\mathrm{d}\theta = \pi\cosh\left[2(\xi+\xi_0)\right],$$

$$\int_0^{2\pi}\frac{1}{M^2}\,\mathrm{d}\theta = \frac{4\pi}{\sinh\left[2(\xi+\xi_0)\right]},$$

$$\int_0^{2\pi}\frac{\cos(2\theta)}{M^2}\,\mathrm{d}\theta = 4\pi\left(\frac{\cosh\left[2(\xi+\xi_0)\right]}{\sinh\left[2(\xi+\xi_0)\right]} - 1\right),$$

$$\int_0^{2\pi}\frac{1}{M^2}\frac{\partial\psi_s}{\partial\theta}\,\mathrm{d}\theta = \int_0^{2\pi}\frac{\psi_s\sin(2\theta)}{M^4}\,\mathrm{d}\theta.$$

The boundary conditions for F_m and G_m are

$$G_m = F_m = F'_m = 0 \quad \text{on} \quad \xi = 0, \tag{3.33}$$

$$G_m, F_m, F'_m \to 0 \quad \text{as} \quad \xi \to \infty. \tag{3.34}$$

These boundary conditions correspond to forcing the disturbances to satisfy the surface boundary conditions found in the previous chapter, and to disappear at large distances from the cylinder.

Thus we see that the stability problem is reduced to solving an eigenvalue problem for $\sigma(m, Gr, Pr, \eta, r)$, the sign of which determines the stability of the system. It is interesting to see that the differential equations for F_m and G_m do not depend explicitly on the parameter Gr, the only dependence on the Grashof number is contained implicitly within the solutions of the flow variables.

Chapter 4

Numerical Solutions

4.1 Steady-State Solution Procedure

To begin the numerical solution of the governing equations, we discretize the computational domain which is bounded by $0 \leq \xi \leq \xi_\infty$ and $0 \leq \theta \leq 2\pi$ into a uniform $N \times L$ grid. Here, ξ_∞ refers to the placement of the outer boundary of the computational domain. The gridpoints are given by

$$\begin{aligned} \xi_i &= ih \qquad i = 0, 1, \ldots, N \\ \theta_j &= jk \qquad j = 0, 1, \ldots, L \end{aligned}$$

where $h \equiv \triangle\xi = \frac{\xi_\infty}{N}$ and $k \equiv \triangle\theta = \frac{2\pi}{L}$.

To discretize the streamfunction equation (2.37) we use a central finite difference scheme. With $\Omega_{i,j} \equiv \Omega(\xi_i, \theta_j)$ where Ω is one of the flow variables ψ, ζ

or ϕ, we replace the derivatives in (2.37) by the following approximations

$$\begin{aligned}\frac{\partial^2\Omega}{\partial\xi^2} &= \frac{\Omega_{i+1,j}-2\Omega_{i,j}+\Omega_{i-1,j}}{h^2}+O(h^2),\\ \frac{\partial^2\Omega}{\partial\theta^2} &= \frac{\Omega_{i,j+1}-2\Omega_{i,j}+\Omega_{i,j-1}}{k^2}+O(k^2),\end{aligned}$$

giving

$$\psi_{i+1,j}+\psi_{i-1,j}+H^2\left(\psi_{i,j+1}+\psi_{i,j-1}\right)-h^2M_{i,j}^2\zeta_{i,j}=2\left(1+H^2\right)\psi_{i,j}, \tag{4.1}$$

where $H=h/k$.

Now since the vorticity and heat equations (2.42) and (2.43) are of the same form, we can write them both as

$$\frac{\partial^2\Omega}{\partial\xi^2}+\frac{\partial^2\Omega}{\partial\theta^2}=a_4\left(\frac{\partial\psi}{\partial\xi}\frac{\partial\Omega}{\partial\theta}-\frac{\partial\psi}{\partial\theta}\frac{\partial\Omega}{\partial\xi}\right)+S.$$

We then apply a generalized second-order discretization scheme given by

$$c_0\Omega_{i,j}=c_1\Omega_{i+1,j}+c_2\Omega_{i-1,j}+c_3\Omega_{i,j+1}+c_4\Omega_{i,j-1}-h^2S_{i,j}, \tag{4.2}$$

where

$$
\begin{aligned}
c_0 &= 2 + 2H^2 + 2\beta \left(\frac{a_4 H}{4}\right)^2 [(\triangle\psi_\theta)^2 + (\triangle\psi_\xi)^2], \\
c_1 &= 1 + \frac{a_4 H}{4} \triangle \psi_\theta + \beta \left(\frac{a_4 H}{4}\right)^2 (\triangle\psi_\theta)^2, \\
c_2 &= 1 - \frac{a_4 H}{4} \triangle \psi_\theta + \beta \left(\frac{a_4 H}{4}\right)^2 (\triangle\psi_\theta)^2, \\
c_3 &= H^2 - \frac{a_4 H}{4} \triangle \psi_\xi + \beta \left(\frac{a_4 H}{4}\right)^2 (\triangle\psi_\xi)^2, \\
c_4 &= H^2 + \frac{a_4 H}{4} \triangle \psi_\xi + \beta \left(\frac{a_4 H}{4}\right)^2 (\triangle\psi_\xi)^2,
\end{aligned}
$$

where

$$
\triangle\psi_\xi = \psi_{i+1,j} - \psi_{i-1,j}, \quad \triangle\psi_\theta = \psi_{i,j+1} - \psi_{i,j-1}.
$$

Here β is a computational parameter which has not yet been defined. A value of $\beta = 0$ will reduce the above system to the usual central-difference scheme, however, in order to ensure diagonal dominance of the resulting matrix, and therefore convergence of an iterative solution method, a value of $\beta \geq 1/4$ is needed. Further explanation for this criteria can be found in Meyer [15]. Such a scheme still has the same second-order accuracy as a central-differencing scheme.

Boundary conditions on the cylinder surface for the streamfunction and temperature are known, but a condition on the surface vorticity is still needed. To find such a condition, we use the Taylor expansion of ψ near the cylinder surface, and the streamfunction equation (2.37) evaluated at the surface. The

Taylor expansion is

$$\psi(\xi = h) = \psi_{0,j} + h\left(\frac{\partial\psi}{\partial\xi}\right)_{0,j} + \frac{h^2}{2}\left(\frac{\partial^2\psi}{\partial\xi^2}\right)_{0,j} + \frac{h^3}{6}\left(\frac{\partial^3\psi}{\partial\xi^3}\right)_{0,j} + O(h^4), \tag{4.3}$$

and equation (2.37) on the surface becomes

$$M_{0,j}^2\zeta_{0,j} = \left(\frac{\partial^2\psi}{\partial\xi^2}\right)_{0,j}. \tag{4.4}$$

If we differentiate the above surface vorticity expression with respect to ξ we find

$$\left(\frac{\partial^3\psi}{\partial\xi^3}\right)_{0,j} = M_{0,j}^2\left(\frac{\partial\zeta}{\partial\xi}\right)_{0,j} + \zeta_{0,j}\left(\frac{\partial M^2}{\partial\xi}\right)_{0,j}. \tag{4.5}$$

We can find numerical expressions for the derivatives in both of the terms on the right side of the previous equation. From the definition of $M(\xi,\theta)$ it is easily seen that

$$\left(\frac{\partial M^2}{\partial\xi}\right)_{0,j} = \sinh 2\xi_0.$$

As well, an equation for the derivative of ζ is given by

$$\left(\frac{\partial\zeta}{\partial\xi}\right)_{0,j} = \frac{4\zeta_{1,j} - \zeta_{2,j} - 3\zeta_{0,j}}{2h}.$$

This formula can be verified by using l'Hopital's rule for a general function $f(x)$:

$$\lim_{h\to 0}\frac{4f(x+h) - f(x+2h) - 3f(x)}{2h}.$$

We can apply l'Hopital's rule to evaluate the limit by differentiating both the numerator and the denominator with respect to h, since they both approach zero:

$$\lim_{h\to 0} \frac{4f'(x+h) - 2f'(x+2h)}{2}.$$

Now letting $x = 0$:

$$\lim_{h\to 0} \frac{4f'(0+h) - 2f'(0+2h)}{2}.$$

Taking the limit then gives

$$\frac{4f'(0) - 2f'(0)}{2} = f'(0),$$

thus

$$f'(0) \equiv f'_0 = \frac{4f_1 - f_2 - 3f_0}{2h}$$

and the above formula for the derivative of ζ holds.

Combining these results with the previously found boundary conditions on the streamfunction, $\psi_{0,j} = \left(\frac{\partial \psi}{\partial \xi}\right)_{0,j} = 0$, the Taylor expansion (4.3) becomes

$$\left(3M_{0,j}^2 + 2h \sinh 2\xi_0\right) \zeta_{0,j} = \frac{12\psi_{1,j}}{h^2} - M_{0,j}^2 \left(4\zeta_{1,j} - \zeta_{2,j}\right) \tag{4.6}$$

which is second-order accurate and will used to determine the surface vorticity.

At the computational outer boundary we must enforce the gradient far-field conditions (3.24) - (3.26). Because of the unknown constants involved in these conditions, we use alternate gradient conditions which agree with (3.24) - (3.26)

but are easier to implement:

$$\begin{aligned} \frac{\partial \psi}{\partial \xi} &= -\psi, \\ \frac{\partial \zeta}{\partial \xi} &= -3\zeta, \\ \frac{\partial \phi}{\partial \xi} &= -4\phi \qquad \text{as} \qquad \xi \to \infty. \end{aligned}$$

To realize these conditions numerically, we recognize that the solution to the first of these gradient conditions corresponds to

$$\psi = ce^{-\xi}$$

for some constant c. At the gridpoints corresponding to the outer boundary this condition becomes

$$\psi_{N,j} = e^{-h}\psi_{N-1,j}. \tag{4.7}$$

Similarly, the conditions for the other flow variables are given by

$$\zeta_{N,j} = e^{-3h}\zeta_{N-1,j}, \tag{4.8}$$

$$\phi_{N,j} = e^{-4h}\phi_{N-1,j}. \tag{4.9}$$

Along the boundaries $\theta = 0$ and $\theta = 2\pi$ (corresponding to $j = 0, L$) periodicity conditions were imposed on the flow variables ψ, ζ, ϕ. That is, equation (4.2) for

$j = 0$ becomes

$$c_0\Omega_{i,0} = c_1\Omega_{i+1,0} + c_2\Omega_{i-1,0} + c_3\Omega_{i,1} + c_4\Omega_{i,L-1} - h^2 S_{i,0},$$

while for $j = L$, (4.2) becomes

$$c_0\Omega_{i,L} = c_1\Omega_{i+1,L} + c_2\Omega_{i-1,L} + c_3\Omega_{i,1} + c_4\Omega_{i,L-1} - h^2 S_{i,L}.$$

We now summarize the numerical method by listing the numerical procedure. An initial form is assumed for all quantities: a zero streamfunction, temperature exponentially decreasing in ξ, and vorticity which is sinusoidal in θ and exponentially decreasing in ξ. We perform the following steps (p denotes the iteration counter) until convergence of a solution: (i) solve for $\psi^{(p)}(\xi_\infty, \theta)$ using equation (4.7), then for $\psi^{(p)}(\xi, \theta)$ through the rest of the domain with equation (4.1) using $\zeta^{(p-1)}$; (ii) solve for $\phi^{(p)}(\xi_\infty, \theta)$ using equation (4.9), then for $\phi^{(p)}(\xi, \theta)$ through the rest of the domain with equation (4.2) using $\psi^{(p)}$; (iii) solve for $\zeta^{(p)}(\xi_\infty, \theta)$ using equation (4.8), $\zeta^{(p)}(0, \theta)$ using equation (4.6), then for $\zeta^{(p)}(\xi, \theta)$ through the rest of the domain with equation (4.2) using $\psi^{(p)}, \phi^{(p)}$; (iv) check convergence: compute maximum absolute difference between $\psi^{(p)}, \phi^{(p)}, \zeta^{(p)}$ and $\psi^{(p-1)}, \phi^{(p-1)}, \zeta^{(p-1)}$, respectively, throughout the computational domain and determine if it is less than a prescribed tolerance ϵ; (v) if convergence is not reached, repeat above steps, incrementing p by 1 after each complete iteration.

4.2 Stability Calculations

To solve the differential equations (3.31) and (3.32) we use the following central-difference derivative approximations:

$$\begin{aligned}
F' &= \frac{F_{i+1} - F_{i-1}}{2h} + O(h^2), \\
F'' &= \frac{F_{i+1} - 2F_i + F_{i-1}}{h^2} + O(h^2), \\
G'' &= \frac{G_{i+1} - 2G_i + G_{i-1}}{h^2} + O(h^2), \\
F''' &= \frac{F_{i+2} - 2F_{i+1} + 2F_{i-1} - F_{i-2}}{2h^3} + O(h^2), \\
F'''' &= \frac{F_{i+2} - 4F_{i+1} + 6F_i - 4F_{i-1} + F_{i-2}}{h^4} + O(h^2),
\end{aligned}$$

where $F_i = F(\xi_i)$, $G_i = G(\xi_i)$ and $h = \xi_{i+1} - \xi_i$ as in the previous section. As well, the coefficient functions $f_1(\xi), f_2(\xi), f_3(\xi), f_4(\xi), g_1(\xi), g_2(\xi)$ are evaluated at ξ_i, and the integrals in the coefficient functions evaluated using Simpson's rule, giving $f_{1,i} = f_1(\xi_i)$, etc.

Making these substitutions for the derivatives in equation (3.31) leads to the system

$$G_{i-1} + \gamma_1 G_i + G_{i+1} + \gamma_2 F_i = 0, \qquad i = 2, 3, \ldots, N-2$$

where γ_1 and γ_2 have implied dependence on i:

$$\begin{aligned}
\gamma_1 &= -2 + g_{1,i} h^2, \\
\gamma_2 &= -g_{2,i} h^2.
\end{aligned}$$

Boundary conditions (3.33) and (3.34) take the form

$$G_0 = F_0 = G_N = F_N = 0$$

which give the equations for $i = 1$ and $i = N - 1$:

$$\gamma_1 G_1 + G_2 + \gamma_2 F_1 = 0,$$

$$G_{N-2} + \gamma_1 G_{N-1} + \gamma_2 F_{N-1} = 0.$$

completing the system of $N - 1$ equations.

Similarly making the derivative substitutions in equation (3.32) and using the boundary conditions (3.33) and (3.34) gives an additional $N - 1$ equations for F:

$$\begin{aligned}
(\beta_1 + \beta_3)F_1 + \beta_4 F_2 + \beta_5 F_3 &= 0, \\
\beta_2 F_1 + \beta_3 F_2 + \beta_4 F_3 + \beta_5 F_4 &= 0, \\
\beta_1 F_{i-2} + \beta_2 F_{i-1} + \beta_3 F_i + \beta_4 F_{i+1} + \beta_5 F_{i+2} &= 0, \qquad i = 3, 4, \ldots, N-3, \\
\beta_1 F_{N-4} + \beta_2 F_{N-3} + \beta_3 F_{N-2} + \beta_4 F_{N-1} &= 0, \\
\beta_1 F_{N-3} + \beta_2 F_{N-2} + (\beta_3 + \beta_5) F_{N-1} &= 0,
\end{aligned}$$

where

$$\begin{aligned}
\beta_1 &= 1 - \tfrac{1}{2} f_{1,i} h, \\
\beta_2 &= -4 + f_{1,i} h + f_{2,i} h^2 - \tfrac{1}{2} f_{3,i} h^3, \\
\beta_3 &= 6 - 2 f_{2,i} h^2 + f_{4,i} h^4, \\
\beta_4 &= -4 - f_{1,i} h + f_{2,i} h^2 + \tfrac{1}{2} f_{3,i} h^3, \\
\beta_5 &= 1 - \tfrac{1}{2} f_{1,i} h.
\end{aligned}$$

We now have a homogeneous $2(N-1) \times 2(N-1)$ nonlinear system of equations for F and G. This system can be written in the form

$$\mathbf{CX} = \mathbf{0}. \tag{4.10}$$

Here $\mathbf{X^T} = (F_1, F_2, \ldots, F_{N-1}, G_1, G_2, \ldots, G_{N-1})$ and $\mathbf{C}$ is the coefficient matix. This coefficient matrix has the form

$$\mathbf{C} = \begin{pmatrix} \mathbf{C_1} & \mathbf{0} \\ \mathbf{C_2} & \mathbf{C_3} \end{pmatrix}$$

where $\mathbf{C_1}, \mathbf{C_2}, \mathbf{C_3}$ are $(N-1) \times (N-1)$ matrices and $\mathbf{0}$ is the $(N-1) \times (N-1)$ zero matrix. It can be seen that the matrices have some symmetry in their forms:

$\mathbf{C_1}$ is pentadiagonal:

$$\mathbf{C_1} = \begin{pmatrix} \beta_1+\beta_3 & \beta_4 & \beta_5 & 0 & 0 & \cdots & \cdots & 0 \\ \beta_2 & \beta_3 & \beta_4 & \beta_5 & 0 & 0 & & \vdots \\ \beta_1 & \beta_2 & \beta_3 & \beta_4 & \beta_5 & 0 & & \\ 0 & \beta_1 & \beta_2 & \beta_3 & \beta_4 & \beta_5 & \ddots & \vdots \\ 0 & 0 & \beta_1 & \beta_2 & \beta_3 & \beta_4 & \ddots & 0 \\ \vdots & 0 & 0 & \beta_1 & \beta_2 & \beta_3 & \ddots & \beta_5 \\ \vdots & & & \ddots & \ddots & \ddots & \ddots & \beta_4 \\ 0 & \cdots & & \cdots & 0 & \beta_1 & \beta_2 & \beta_3+\beta_5 \end{pmatrix};$$

$\mathbf{C_2}$ is diagonal:

$$\mathbf{C_2} = \begin{pmatrix} \gamma_2 & 0 & \cdots & 0 \\ 0 & \gamma_2 & \ddots & \vdots \\ \vdots & \ddots & \ddots & 0 \\ 0 & \cdots & 0 & \gamma_2 \end{pmatrix};$$

and $\mathbf{C_3}$ is tridiagonal:

$$\mathbf{C_3} = \begin{pmatrix} \gamma_1 & 1 & 0 & \cdots & 0 \\ 1 & \gamma_1 & 1 & 0 & \vdots \\ 0 & 1 & \gamma_1 & \ddots & \\ \vdots & 0 & \ddots & \ddots & 1 \\ 0 & \cdots & & 1 & \gamma_1 \end{pmatrix}.$$

In order to have a nontrivial solution to equation (4.10) we must enforce the condition

$$\det(\mathbf{C}) = 0. \tag{4.11}$$

Since

$$\det\begin{pmatrix} \mathbf{C_1} & \mathbf{0} \\ \mathbf{C_2} & \mathbf{C_3} \end{pmatrix} = \det(\mathbf{C_1})\det(\mathbf{C_3}),$$

the equations (3.32) and (3.31) can be decoupled. Equation (4.11) then becomes

$$\det(\mathbf{C_1}) = 0 \quad \text{and/or} \quad \det(\mathbf{C_3}) = 0. \tag{4.12}$$

Solving (4.12) creates a dispersion relation for the growth rate σ, where $\sigma = \sigma(m, Gr, Pr, \eta, r)$. The roots of the polynomials given by (4.12) can be found numerically, giving a method for finding σ for a given m, Gr, Pr, η, r. Of all such roots found, the one with the largest real part is the most significant, as this corresponds to the most unstable mode.

4.2.1 Müller's Method

In order to solve the dispersion relation given by equations (4.12) a method is needed to find complex roots of a polynomial. Müller's method, which is described fully in [3], is an extension of the Secant method and gives such a procedure.

In this method we look for the roots of a function $f(x)$ (in our case, this will be the determinant as a function of σ) that, near an intersection with the

x-axis, passes through three points $(x_0, f(x_0)), (x_1, f(x_1))$, and $(x_2, f(x_2))$. This function is approximated by a parabola whose root corresponds with the function's intersection with the x-axis, and the parabola is given by a polynomial with the form

$$P(x) = a(x - x_2)^2 + b(x - x_2) + c.$$

Since the parabola passes through the three points $(x_0, f(x_0)), (x_1, f(x_1))$, and $(x_2, f(x_2))$, we have

$$\begin{aligned} f(x_0) &= a(x_0 - x_2)^2 + b(x_0 - x_2) + c, \\ f(x_1) &= a(x_1 - x_2)^2 + b(x_1 - x_2) + c, \\ f(x_2) &= c. \end{aligned}$$

These equations can be solved to find the coefficients a, b, c in terms of the three points $(x_0, f(x_0)), (x_1, f(x_1))$, and $(x_2, f(x_2))$, giving

$$a = \frac{(x_1 - x_2)[f(x_0) - f(x_2)] - (x_0 - x_2)[f(x_1) - f(x_2)]}{(x_0 - x_2)(x_1 - x_2)(x_0 - x_1)}, \tag{4.13}$$

$$b = \frac{(x_0 - x_2)^2[f(x_1) - f(x_2)] - (x_1 - x_2)^2[f(x_0) - f(x_1)]}{(x_0 - x_2)(x_1 - x_2)(x_0 - x_1)}, \tag{4.14}$$

$$c = f(x_2). \tag{4.15}$$

We now have the coefficients of $P(x)$ in terms of the given points. To then determine the root of the polynomial, x_3, we need to solve $P(x) = 0$. If we do this by applying the quadratic formula in a straightforward way, one of the roots we

find is

$$x - x_2 = \frac{-b + \sqrt{b^2 - 4ac}}{2a}$$

which involves subtracting two numbers which could be nearly equal if $b^2 \gg 4ac$. To avoid the errors that this would incur, we rationalize the numerator:

$$x - x_2 = \frac{-b + \sqrt{b^2 - 4ac}}{2a}\left(\frac{-b - \sqrt{b^2 - 4ac}}{-b - \sqrt{b^2 - 4ac}}\right) = \frac{-2c}{b + \sqrt{b^2 - 4ac}}.$$

Performing a similar rationalization on the other root found by the quadratic formula, we have the roots of $P(x)$ given by

$$x_3 - x_2 = \frac{-2c}{b \pm \sqrt{b^2 - 4ac}}.$$

In order to choose x_3 to be the root which is closest to x_2, we maximize the denominator in the above equation by choosing the sign of the radical term according to the sign of b. Thus, the root is found by

$$x_3 = x_2 - \frac{2c}{b + \mathrm{sgn}(b)\sqrt{b^2 - 4ac}},$$

where a, b, and c are given by equations (4.13) - (4.15).

Once x_3 is found, Müller's method is repeated with initial points now given by x_1, x_2, x_3 to find x_4, the next approximation to the intersection value of the function $f(x)$. The method is repeated until the roots found in two successive

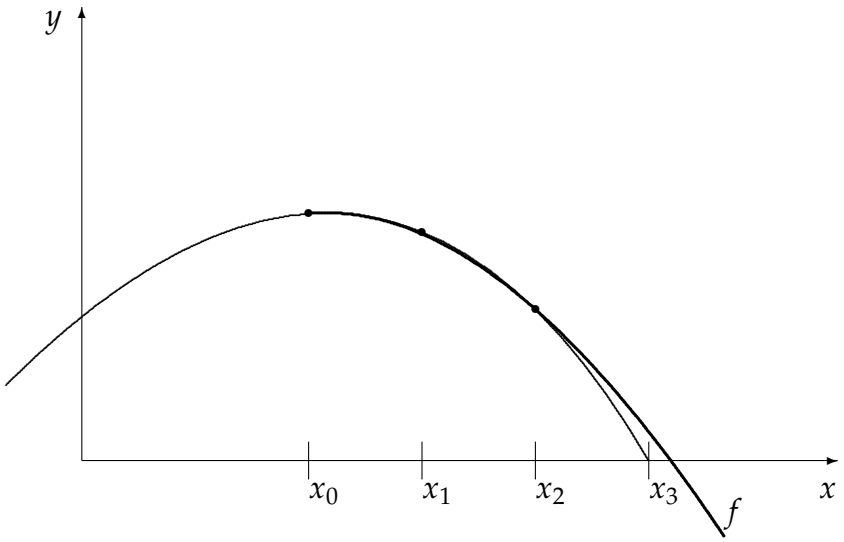

Figure 4.1: Müller's method for polynomial root-finding

iterates are within a tolerance ϵ.

Convergence for Müller's method is generally fast for any initial starting values. In our case, the only drawback to using this method is related to the large number of roots in our function. The determinant function of σ has $N-1$ roots, and we are only interested in the single root with the largest real part. One solution is to implement a deflationary method to reduce the order of the determinant function once a root is found. However, such a method depends on repeated approximations, and the compounding errors would become unmanageable. Instead, manual repetitions of Müller's method are performed until it becomes clear that the largest root has been found.

Chapter 5

Results

Presented in this chapter are detailed numerical results obtained by the methods described in previous chapters. The problem of free convection from an inclined elliptic cylinder is completely characterized by the parameters r, η, Gr, Pr. Solutions were obtained for parameter values $\eta = 0, \frac{\pi}{4}, \frac{\pi}{2}$, $r = 0.2, 0.5, 0.8$, $1 \leq Pr \leq 10$, and $1 \leq Gr \leq 10$.

5.1 Steady State

To begin the numerical simulations the following initial guess was used for a given r, η, Pr and $Gr = 1$:

$$\phi = e^{-\xi}, \tag{5.1}$$

$$\psi = 0, \tag{5.2}$$

$$\zeta = 0.1e^{-\xi^2} \sin\theta. \tag{5.3}$$

The initial temperature corresponds to $\phi = 1$ on the cylinder surface and then exponentially decreasing through the flow field. The fluid being initially at rest leads to the choice of a zero streamfunction as a first guess. Having a small sinusoidal vorticity around the cylinder, decreasing exponentially away from the surface, was used because it has been shown in previous work (D'Alessio and Williams, [6]) that the surface vorticity is roughly sinusoidal in form.

As is usual with problems of this type, under-relaxation was implemented in calculating the surface vorticity. In the generalized finite difference scheme (4.2), the value $\beta = 1/2$ was used. It was found that a value of $\beta = 0$, which corresponds to using the central finite difference scheme, led to difficulties with convergence.

Once convergence was obtained for a specified r, η, Pr and $Gr = 1$, this solution was then used as an initial guess for $Gr = 5$. The solution obtained from this was then used as an initial guess for $Gr = 10$. This gradual stepping of the Grashof number helped the convergence process.

The appropriate boundary placement using the gradient far-field conditions was determined by numerous trial runs. Values of $\xi_\infty = 3, 3.5$ and 4 were used, corresponding to outer boundary locations of about 18, 27 and 45 semi-major axis lengths away from the body, respectively. As can be seen in Figure 5.1, there is little variation in the surface vorticity with the different outer boundary placements. We can also use the average Nusselt number, $\overline{Nu}$, to compare results. The Nusselt number is a dimensionless measure of the surface heat

flux, so the average surface Nusselt number is given by

$$\overline{Nu} = \frac{1}{2\pi}\int_{-\pi}^{\pi} Nu \, \mathrm{d}\theta \quad \text{where} \quad Nu = -2\left(\frac{1}{M}\frac{\partial \phi}{\partial \xi}\right)_0 .$$

Here, $\overline{Nu}$ has values of 1.469, 1.489, and 1.497, respectively, for the three boundary placements. It was found that using a value of $\xi_\infty = 3.5$ was sufficient and moving to a farther boundary placement produced no significant difference. All further simulations use this value, with a grid of $N \times L = 71 \times 121$. Convergence was defined when the absolute value of two successive iterates of the streamfunction, temperature, vorticity and Nusselt number differed by less than a tolerance ϵ. A value of $\epsilon = 10^{-5}$ was typically used.

Two possible conditions at the outer boundary could be implemented: the zero boundary condition discussed in Section 2.4, or the gradient far-field conditions found in Chapter 3 using asymptotic analysis. Figure 5.2 shows the Nusselt number distribution along the cylinder surface using the different boundary conditions, as well as that for the long-time unsteady case for comparison. It is clear that, while all three cases give similar results, the gradient conditions yields better agreement with the long-time unsteady case, which suggests that these are more suitable conditions.

Figure 5.3 shows the isotherms for the two types of boundary conditions. Shown are the contours $\phi = 0.1, \ldots, 1$ in increments of $\triangle\phi = 0.1$. The outermost contour corresponds to $\phi = 0.1$ and the innermost to $\phi = 1$, that is, the cylinder surface. It is seen that the contours close to the cylinder surface are

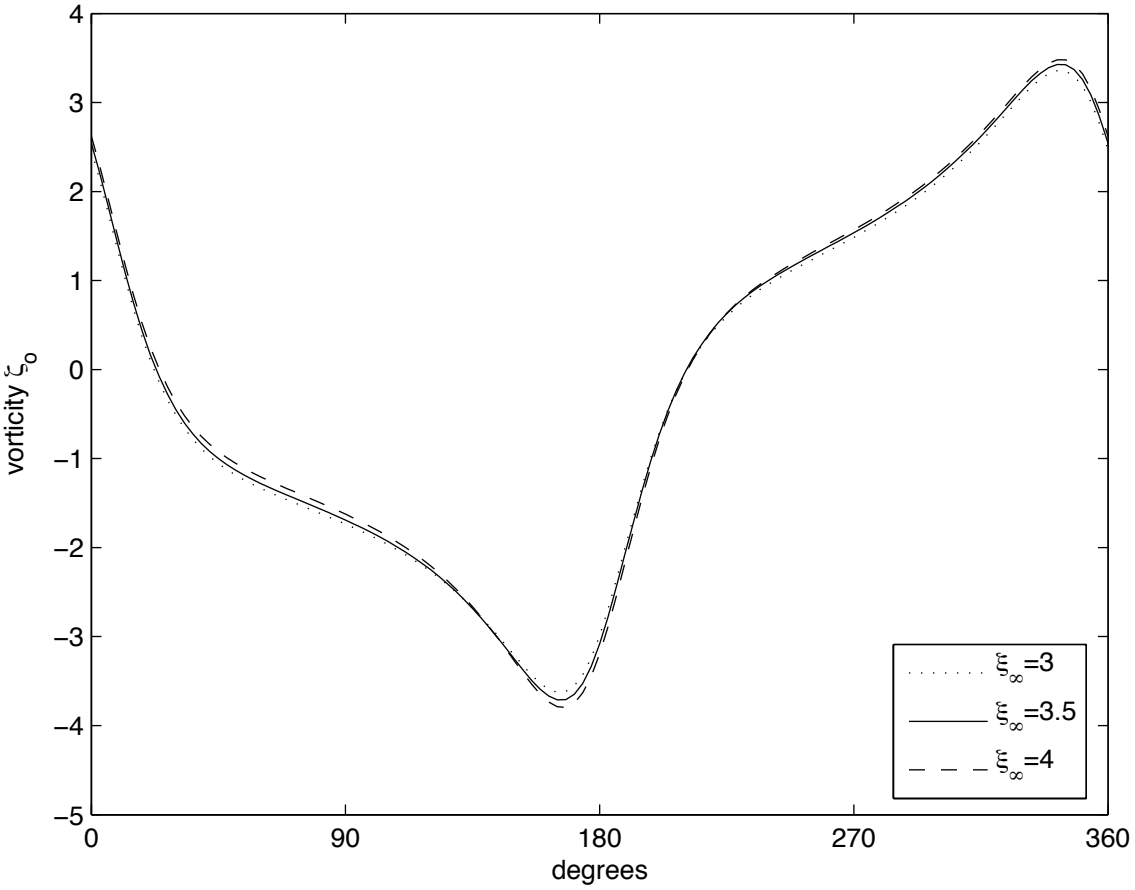

Figure 5.1: Surface vorticity demonstrating outer boundary placement ($\eta = 45^0, Gr = 1, Pr = 1, r = 0.5$)

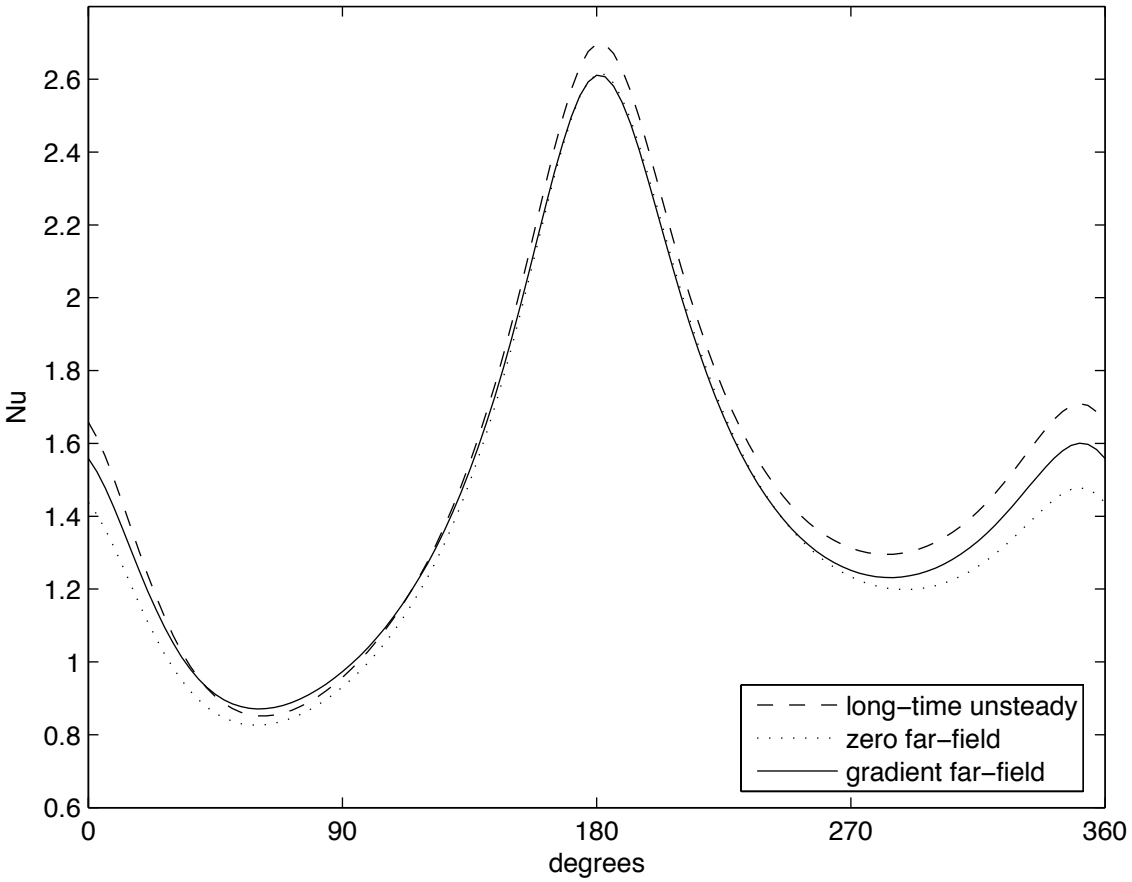

Figure 5.2: Nusselt number distribution demonstrating boundary conditions
($\eta = 45^0, Gr = 1, Pr = 1, r = 0.5$)

very similar in both cases, but there are large differences far from the surface. The mushrooming seen when zero boundary conditions are used is a result of the compression of the flow field, while the more plume-like structure seen with the gradient far-field conditions is physically more realistic. This further supports the use of the gradient conditions at the outer boundary over the zero conditions.

In Figure 5.4 we see the streamlines for this case with the gradient boundary conditions. Here the lines of constant streamfunction are plotted for $\psi = -15 \cdots -3$ in steps of $\triangle\psi = 1$, $\psi = -3 \cdots -1$ in steps of $\triangle\psi = 0.5$, $\psi = -1 \cdots 1$ in steps of $\triangle\psi = 0.25$, $\psi = 1 \cdots 3$ in steps of $\triangle\psi = 0.5$, and $\psi = 3 \cdots 15$ in steps of $\triangle\psi = 1$. The streamlines show the paths of the fluid particles; the fluid is seen to rise above the cylinder and descend farther to the sides in a recirculating flow pattern.

Figure 5.5 shows the streamlines for the unsteady case at a dimensionless time of $t = 29.5$. A pocket of higher temperature fluid is seen above the cylinder; as these solutions are integrated further in time this particular pocket dissipates, and new such pockets are formed. This repeated formation of heated areas indicates an instability in the flow.

Having thus determined the appropriate outer boundary placement and far-field condition, results were found for various values of η, r, Pr and Gr. Figure 5.6 shows the isotherms for $\eta = 0$. The isotherm plot for $\eta = \frac{\pi}{2}$ is very similar. As may be expected for these symmetric cases, the plumes are more vertically upright than those in the $\eta = \frac{\pi}{4}$ case. Table 5.1 lists the average Nusselt

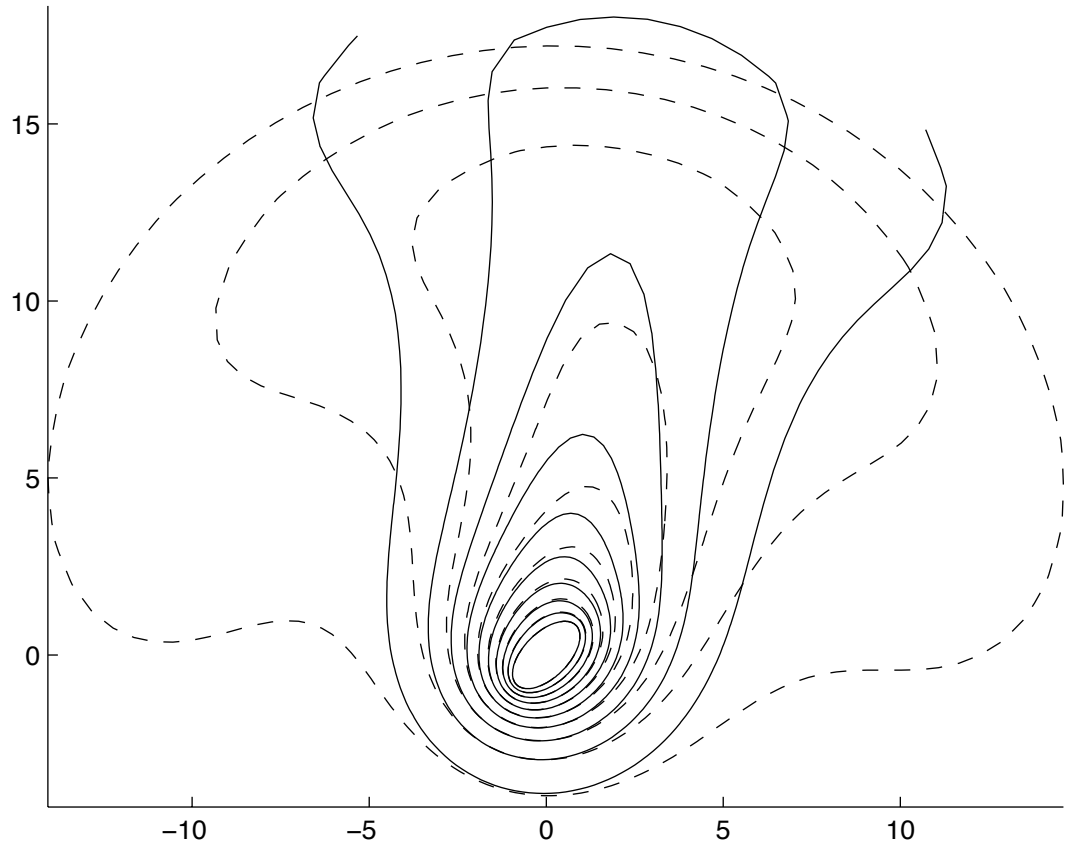

Figure 5.3: Isotherms demonstrating boundary conditions
($\eta = 45^0, Gr = 1, Pr = 1, r = 0.5$). Solid line represents gradient conditions, dashed line represents zero conditions.

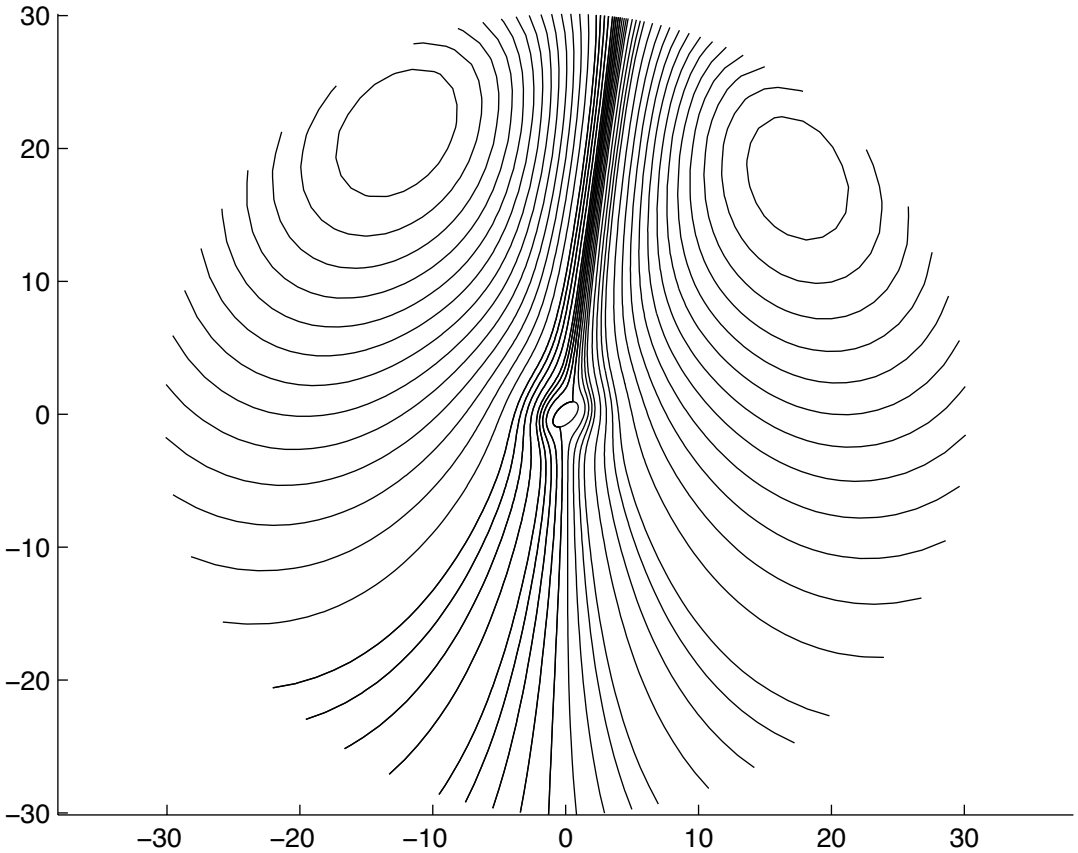

Figure 5.4: Streamlines for $\eta = 45^0$, $Gr = 1$, $Pr = 1$, $r = 0.5$

	$\overline{Nu}$		
η	$Gr = 1$	$Gr = 5$	$Gr = 10$
0	1.468	1.902	2.125
$\frac{\pi}{4}$	1.489	1.925	2.167
$\frac{\pi}{2}$	1.510	1.962	3.333

Table 5.1: Average Nusselt numbers for various Grashof numbers and inclinations with $Pr = 1$ and $r = 0.5$

numbers for various η and Gr with $Pr = 1$ and $r = 0.5$.

Figures 5.7 and 5.8 plot the surface vorticity and Nusselt number distribution, respectively, for three different Grashof numbers: $Gr = 1, 5$, and 10. We see that with increasing Grashof number, that is, with increasingly stronger buoyancy forces compared with viscous forces, there is a marked increase in magnitude of surface vorticity with pronounced variations occurring near the tips of the cylinder. The Nusselt distributions show a general increase in surface heat flux with increasing Grashof number. Figure 5.9 contrasts the isotherms for $Gr = 1$ (solid line) and $Gr = 10$ (dashed line). Again we see the effect of increased buoyancy, here by the narrowing of the plume. This effect is also observed in the streamline plots, Figures 5.4, 5.10 and 5.11. The spacing between consecutive streamlines is noticeably reduced in Figure 5.11 which indicates larger gradients and hence larger velocities brought on by the stronger buoyancy force. The same argument can be applied to the spacing between consecutive isotherms which can be related to the rate of heat transfer. In these plots the lines of constant streamfunction are presented for $\psi = -28 \cdots 26$ in the $Gr = 5$ case, and $\psi = -35 \cdots 32$ for $Gr = 10$ with similar spacing as in Figure 5.4. Average Nusselt numbers for these cases can be found in Table 5.1: the

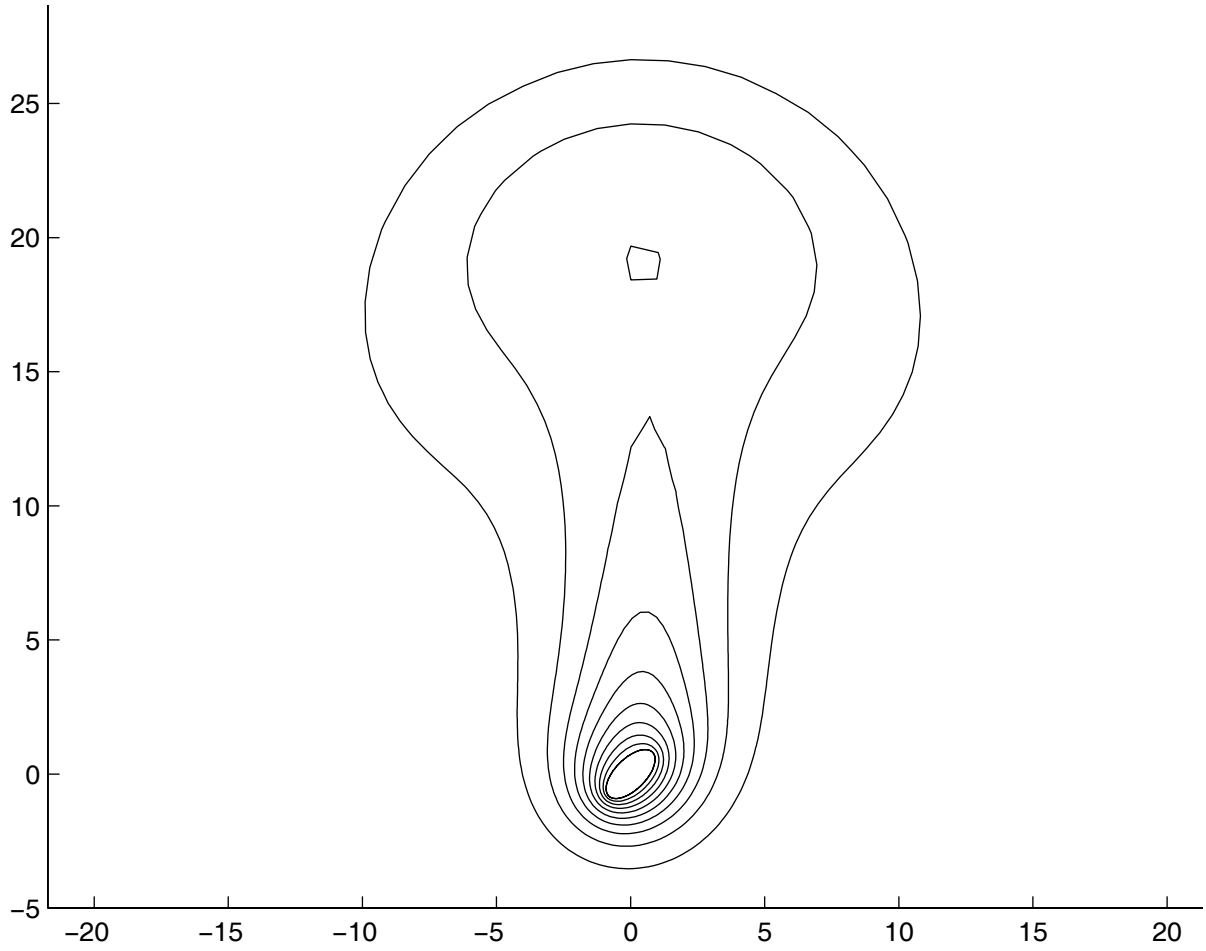

Figure 5.5: Isotherms for the unsteady case, with $\eta = 45^0$, $Gr = 1$, $Pr = 1$, $r = 0.5$ at a dimensionless time of $t = 29.5$

	$\overline{Nu}$		
r	$Gr = 1$	$Gr = 5$	$Gr = 10$
0.2	2.008	2.544	2.836
0.5	1.489	1.925	2.167
0.8	1.096	1.455	1.655

Table 5.2: Average Nusselt numbers for various Grashof numbers and aspect ratios with $Pr = 1$ and $\eta = \frac{\pi}{4}$

	$\overline{Nu}$		
Pr	$Gr = 1$	$Gr = 5$	$Gr = 10$
1	1.489	1.925	2.167
5	2.096	2.780	3.162
10	2.450	3.267	3.737

Table 5.3: Average Nusselt numbers for various Grashof numbers and Prandtl numbers with $r = 0.5$ and $\eta = \frac{\pi}{4}$

increasing $\overline{Nu}$ for higher Gr indicates a higher rate of heat transfer across the cylinder surface as the buoyancy force increases.

Further results for variations in the ellipse parameter, r, and Prandtl number, Pr, are listed in Tables 5.2 and 5.3. The dependence of $\overline{Nu}$ on the parameters η, r, Gr, and Pr is thus clear: for fixed η and r, the average Nusselt number increases as either Gr or Pr increases. $\overline{Nu}$ decreases as r is increased when Gr, Pr and η are held constant. As well, $\overline{Nu}$ increases as the cylinder rotates from horizontal ($\eta = 0$) to vertical ($\eta = \frac{\pi}{2}$).

Shown in Figure 5.12 are isotherms for a different Prandtl number, $Pr = 10$. Raising the Prandtl number increases the effect of the momentum diffusivity over thermal diffusivity and comparing with Figure 5.3 this effect is observed in the narrowing of the heat plume, a similar effect to increasing the Grashof number.

Figures 5.13 and 5.14 show isotherms for a smaller ellipse aspect ratio, $r = 0.2$. The first of these figures shows that a thinner ellipse enhances the effect of inclination of the cylinder: the plume is more in line with the major axis of the ellipse. Increasing the Grashof number to $Gr = 10$ as shown in Figure 5.14 is equivalent to increasing the strength of buoyancy in the system. Examining the two plots closely reveals that the plume for the higher Grashof number case is more vertically upright than that of the lower Gr. This demonstrates that having stronger buoyancy reduces the asymmetry of the flow.

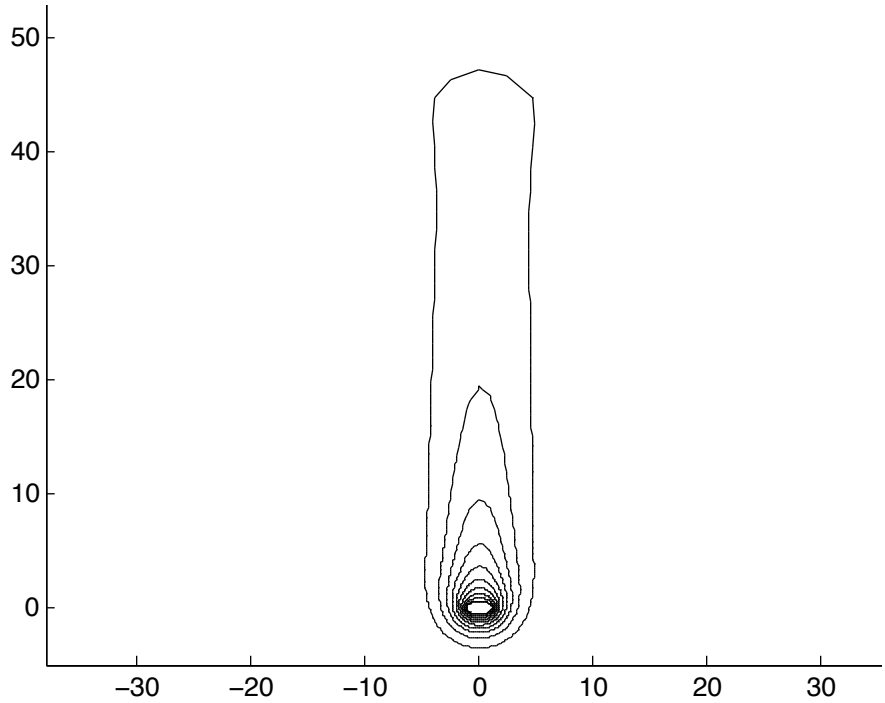

Figure 5.6: Isotherms for $\eta = 0^0$, $Gr = 1$, $Pr = 1$, $r = 0.5$

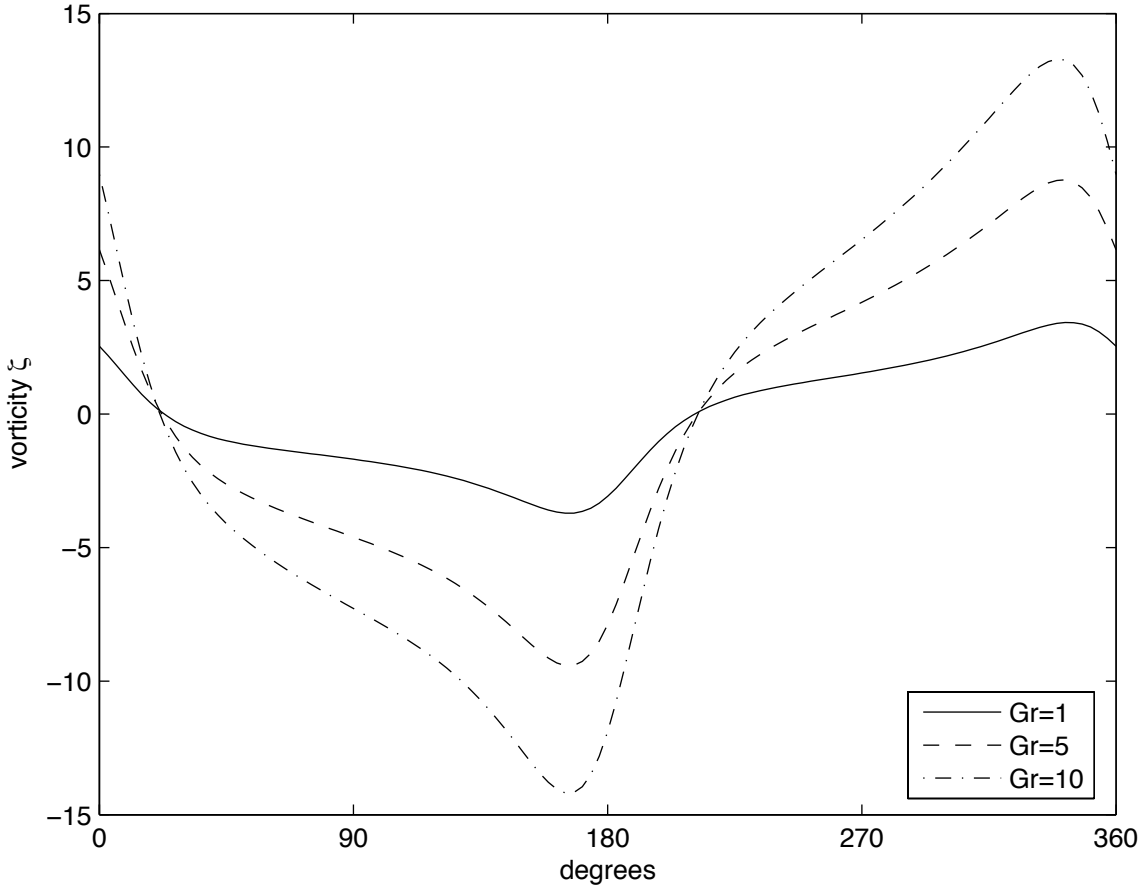

Figure 5.7: Surface vorticity for differing Grashof numbers
($\eta = 45^0, Pr = 1, r = 0.5$)

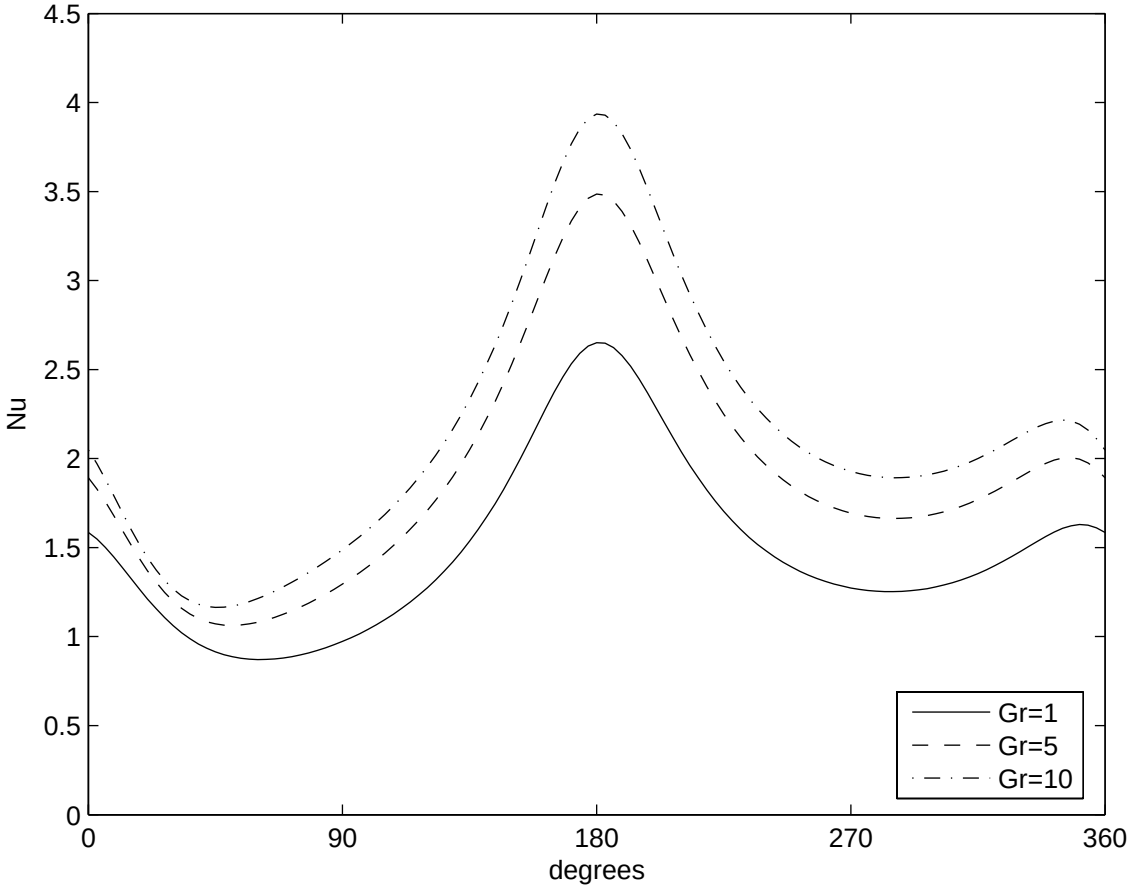

Figure 5.8: Nusselt distribution for differing Grashof numbers
($\eta = 45^0, Pr = 1, r = 0.5$)

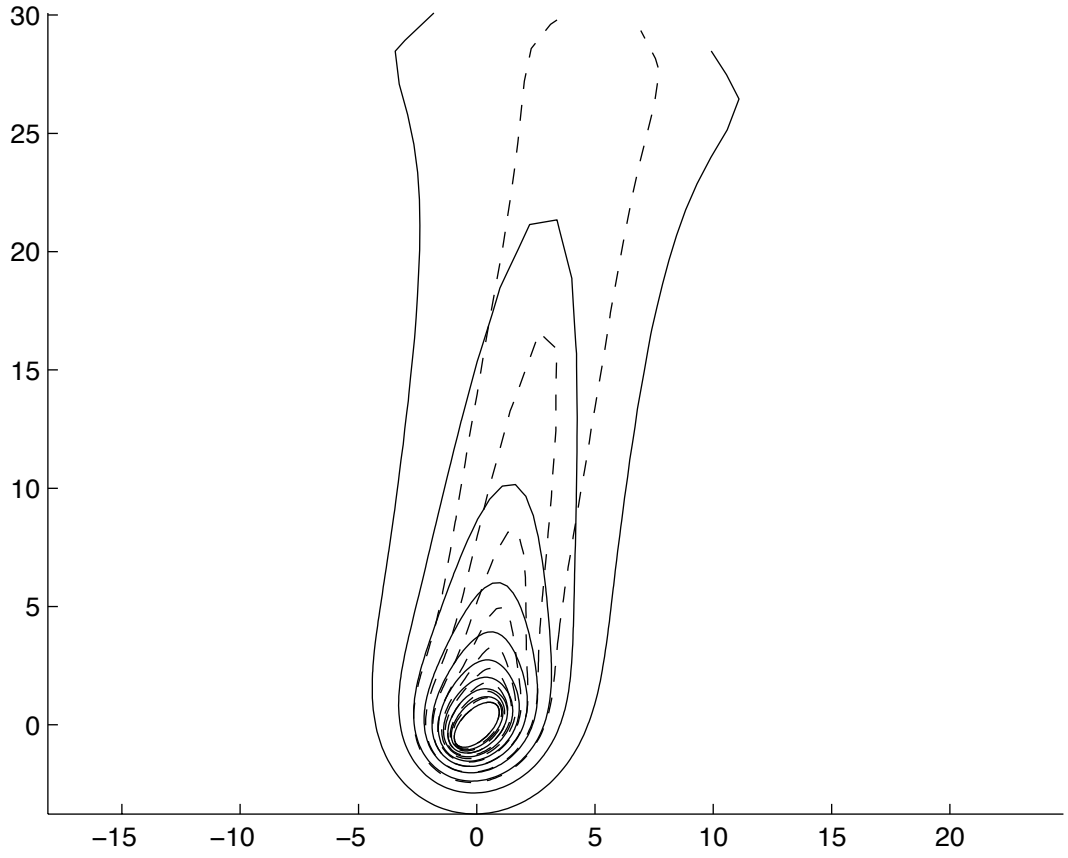

Figure 5.9: Isotherms for $Gr = 1, 10$ ($\eta = 45^0, Pr = 1, r = 0.5$). Solid line represents $Gr = 1$, dashed line represents $Gr = 10$.

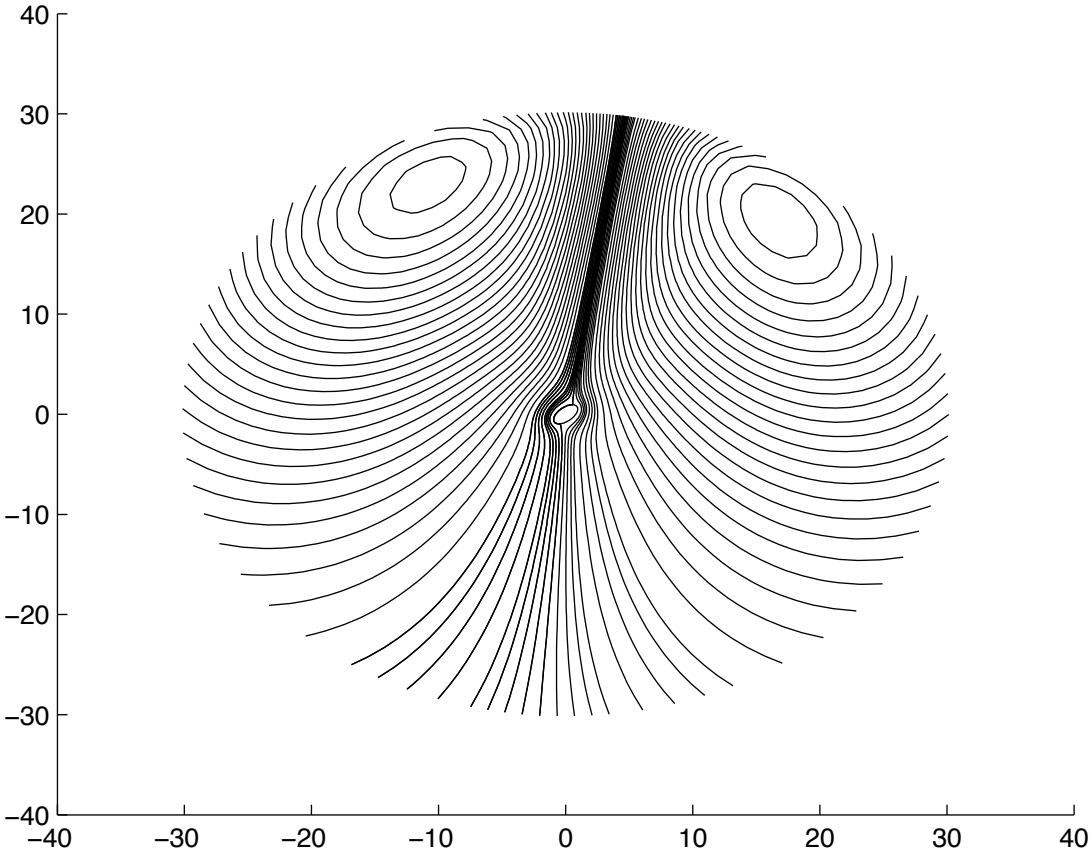

Figure 5.10: Streamlines for $\eta = 45^0$, $Gr = 5$, $Pr = 1$, $r = 0.5$

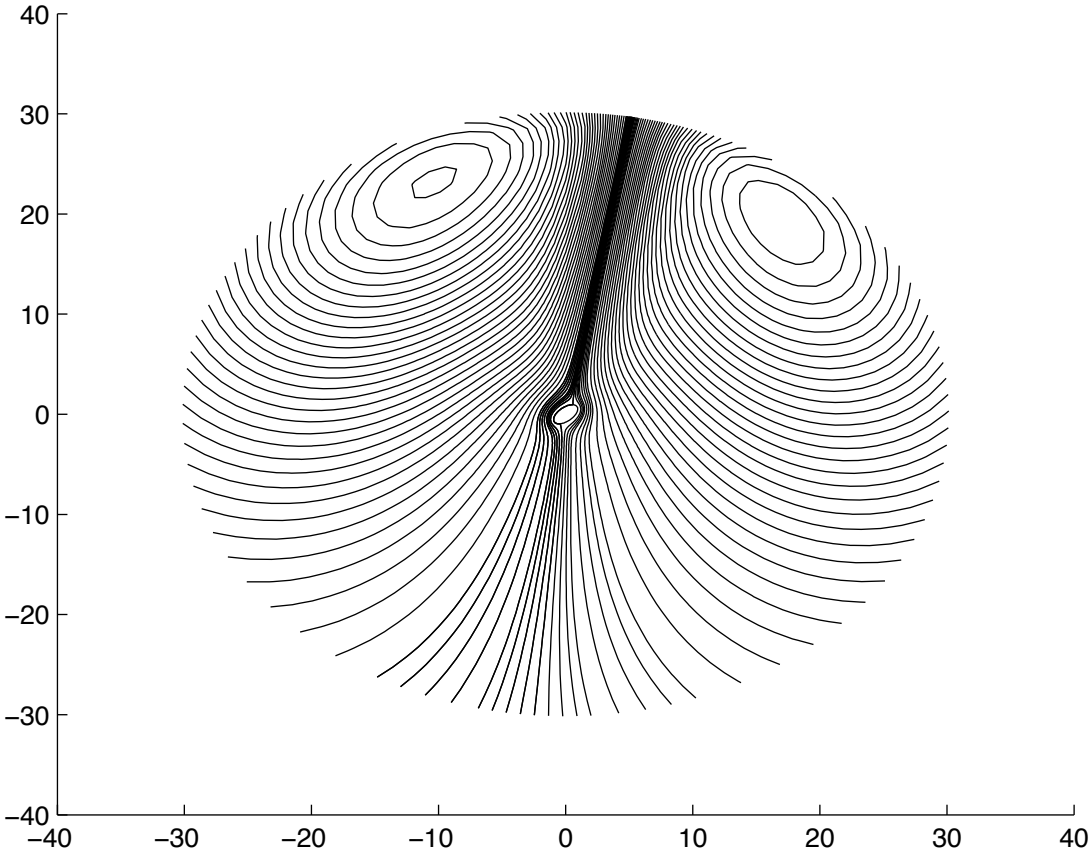

Figure 5.11: Streamlines for $\eta = 45^0$, $Gr = 10$, $Pr = 1$, $r = 0.5$

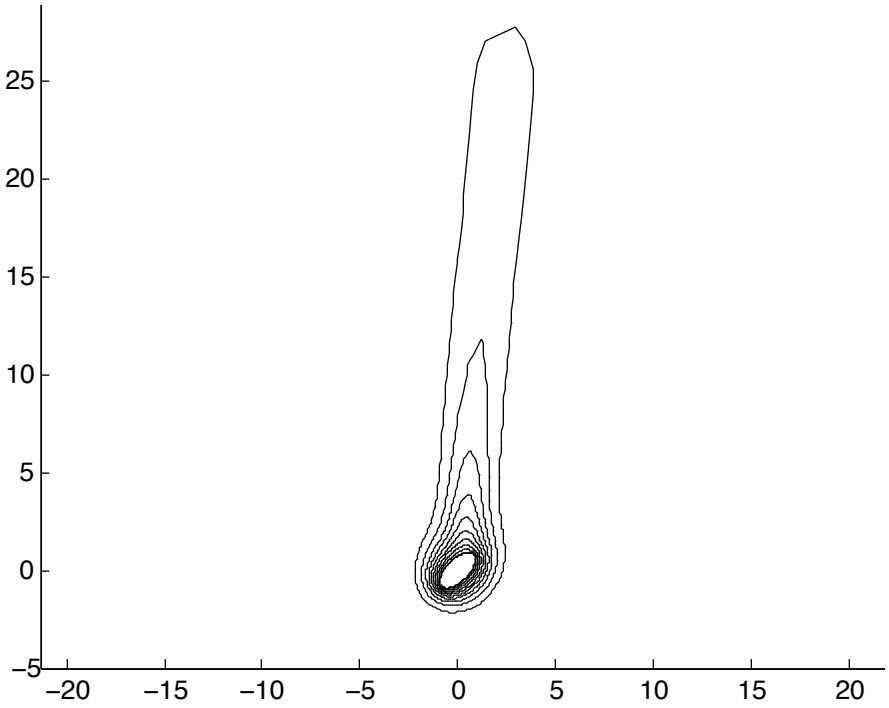

Figure 5.12: Isotherms for $\eta = 45^0$, $Gr = 1$, $Pr = 10$, $r = 0.5$

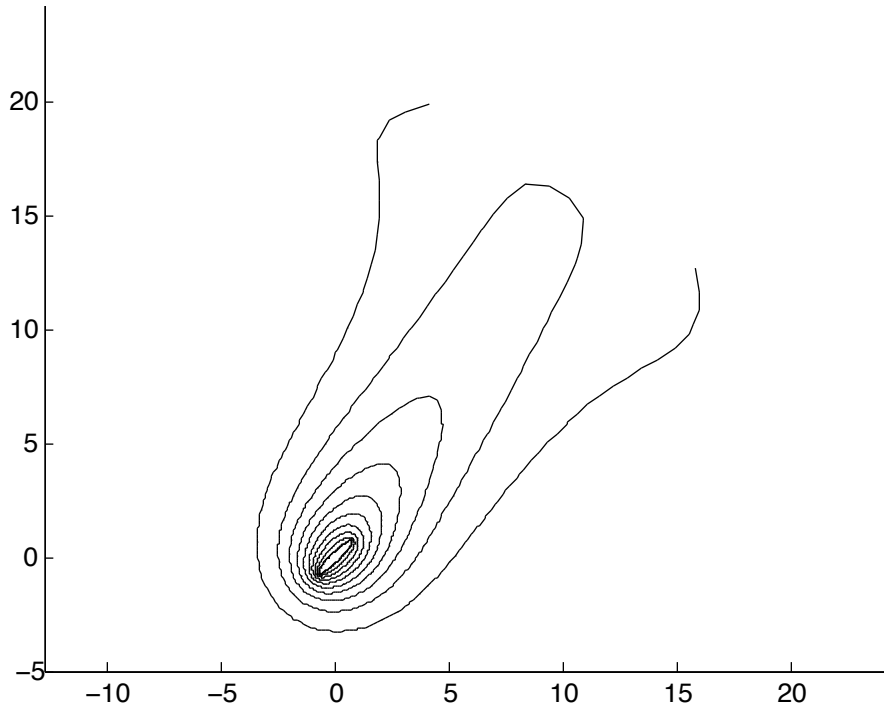

Figure 5.13: Isotherms for $\eta = 45^0$, $Gr = 1$, $Pr = 1$, $r = 0.2$

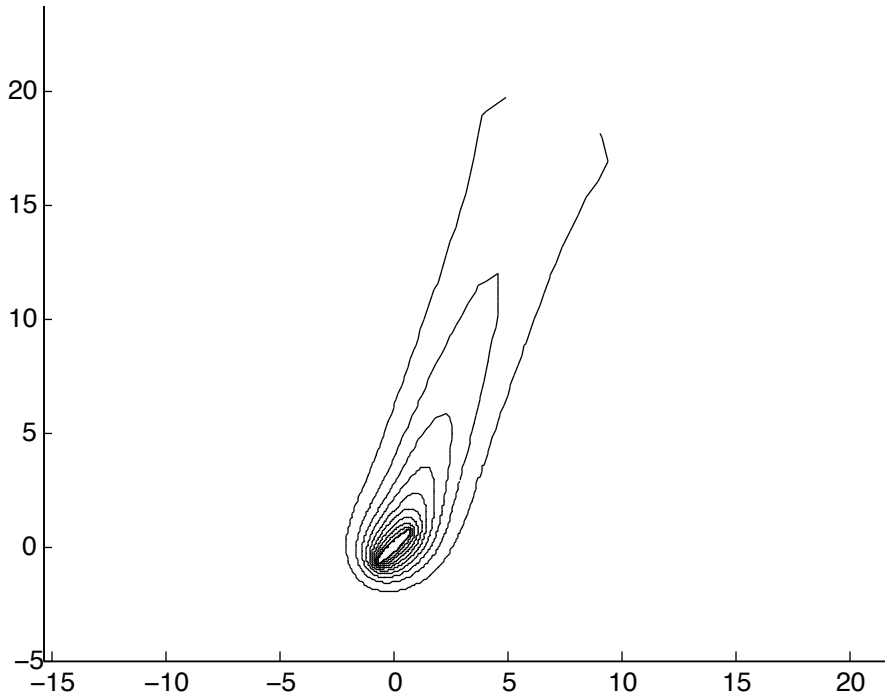

Figure 5.14: Isotherms for $\eta = 45^0$, $Gr = 10$, $Pr = 1$, $r = 0.2$

5.2 Linear Stability

The goal of the linear stability analysis is to estimate the critical Grashof number at which the flow, for a fixed aspect ratio r, inclination η, Prandtl number Pr and mode m, becomes unstable. It was found that the real part of the largest growth rate increased as the mode m decreased, so the most unstable mode corresponds to $m = 0$. However, this largest growth rate was always found to have a negative real part, indicating that the flow was always stable.

It was found that varying the Grashof number or cylinder inclination in the stability analysis did not have any impact on the real part of the largest growth rate. This is a reasonable result, as the stability equations (3.31) - (3.32) do not depend directly on Gr or η. The only dependence on these parameters occurs implicitly in the solutions of ψ, ζ and ϕ. The growth rate was seen to depend mildly on the Prandtl number and the aspect ratio of the cylinder, but the strongest dependence was on the placement of the outer boundary. The observed trend was that the real part of the largest growth rate increased the farther out ξ_∞ was placed, without becoming positive. This result agrees with the observed unsteady flow patterns which suggest that an instability in the flow occurs far away from the cylinder surface, as seen in Figure 5.5, thus the increasing instability of the steady flow with increased ξ_∞. The contradiction between the steady-state stability results and the unsteady flow patterns may reflect the limitations of the linear stability analysis conducted here, but more likely is the result of simplifying the perturbation equations by approximating

each term by a single term of its Fourier series expansion.

Chapter 6

Summary

This work presented steady-state solutions to the problem of free convection from an inclined elliptic cylinder. Asymptotically derived far-field conditions were used in conjunction with numerical schemes involving finite differencing to solve the full steady-state Navier-Stokes and thermal energy equations. Results were found for small to moderate Grashof and Prandtl numbers.

A linear stability analysis was carried out, attempting to determine the critical parameter values (specifically Grashof number) at which the flow became unstable. Instead, for all cases considered, the flow was found to be stable.

Connections were made to corresponding limiting unsteady results. It was observed that comparisons in flow characteristics, such as Nusselt number and surface vorticity, between the steady and long-time unsteady cases were in good agreement. However, the long-time unsteady results revealed instabilities in the form of heat pockets far from the cylinder surface, as shown in Figure (5.5), that were not present in the steady solutions.

An obvious extension of this work is to examine the case of constant heat flux from the cylinder surface instead of the isothermal, or constant temperature, case considered here.

Bibliography

[1] H. M. Badr. Laminar natural convection from an elliptic tube with different orientations. *Journal of Heat Transfer*, 1997.

[2] H. M. Badr and K. Shamsher. Free convection from an elliptic cylinder with major axis vertical. *International Journal of Heat and Mass Transfer*, 1993.

[3] Richard L. Burden and J. Douglas Faires. *Numerical Analysis*. Thompson Learning, seventh edition, 2001.

[4] Louis C. Burmeister. *Convective Heat Transfer*. Wiley, second edition, 1993.

[5] S. J. D. D'Alessio and D. L. Harmsworth. Forced convective heat transfer for an accelerating elliptic cylinder. part 2: Numerical results. In *Proceedings of the 18th Canadian Congress of Applied Mechanics*, 2001.

[6] S. J. D. D'Alessio and M. L. Williams. Free convection from an inclined elliptic cylinder. part 1: Analytical results. In *Proceedings of the 12th An-*

nual Conference of the Computational Fluid Dynamics Society of Canada CFD 2004, 2004.

[7] S. J. D. D'Alessio and M. L. Williams. Free convection from an inclined elliptic cylinder. part 2: Numerical results. In *Proceedings of the 12th Annual Conference of the Computational Fluid Dynamics Society of Canada CFD 2004*, 2004.

[8] S. C. R. Dennis and L. Quartapelle. Some uses of Green's theorem in solving the navier-stokes equations. *International Journal of Numerical Methods in Fluid Dynamics*, 1989.

[9] P. G. Drazin and W. H. Reid. *Hydrodynamic Stability*. Cambridge University Press, 1981.

[10] A. O. Elsayed, E. Z. Ibrahim, and S. A. Elsayed. Free convection from a constant heat flux elliptic tube. *Energy Conversion and Management*, 2003.

[11] P. K. Kundu. *Fluid Mechanics*. Academic Press, second edition, 1990.

[12] F. M. Mahfouz. Natural convection from an elliptic tube with major axis horizontal and placed in a micropolar fluid. *International Journal of Heat and Mass Transfer*, 2004.

[13] W. H. McAdams. *Heat Transmission*. McGraw-Hill, 1954.

[14] J. H. Merkin. Free convection boundary layers on cylinders of elliptic cross-section. *ASME Jounral of Heat Transfer*, 1977.

[15] C. D. Meyer. *Matrix analysis and applied linear algebra*. Society for Industrial and Applied Mathematics, 2000.

[16] T. Saitoh, T. Sajiki, and K. Maruhara. Bench mark solutions to natural convection heat transfer problem around a horizontal circular cylinder. *International Journal of Heat and Mass Transfer*, 1993.

[17] M. G. Saunders. Initial stages of mixed convective heat transfer past an accelerating inclined elliptic cylinder. Master's thesis, University of Waterloo, 2002.

[18] Francis J. Suriano and Kwang-Tzu Yang. Laminar free convection about vertical and horizontal plates at small and moderate Grashof numbers. *International Journal of Heat and Mass Transfer*, 1968.